THE UNIVERSITY OF BIRMINGHAM
Department of Metallurgy and Materials

UNIVERSITY OF BIRMINGHAM

Stiffness variation in hockey sticks and the impact on stick performance

Graeme Nigel Carlisle

788002

Submitted for the degree of

Masters of Research – Science and Engineering of Materials

August 2011

Department of Metallurgy and Materials

Stiffness variation in hockey sticks and the impact on stick performance

Graeme Nigel Carlisle

Submitted with corrections for the degree of
Masters of Research – Science and Engineering of Materials

August 2011

Multiple sectioned shafts of carbon fibre composite were modelled using Composite Design Analysis software in order to replicate the range of flexural rigidities shown across the current field hockey stick market. The shafts were then manufactured using hand lay-up and hot-pressing techniques, tested under static and dynamic conditions and the goodness of their relationship with the modelled behaviour was assessed. The shafts were also analysed microscopically for volume fraction, ply-orientation and the interaction between the varied lay-up sections.

The modelling gave a good understanding of the trend of behaviour that was to be expected, but was not accurate enough to predict experimental values. It is possible to create multiple sectioned CFRP shafts that can be controlled for overall flexural rigidity and also strain distribution or "kick-point". The hand lay-up and hot pressing technique produces consistent volume fraction and accurate fibre orientation, however the seams at which the sections join requires further investigation and development. The relationship between stick stiffness and ball speed validated previous research, stiffer shafts produced a higher CoR in the drop ball test.

There is scope to introduce this stiffness control of the bending behaviour into hockey sticks, by either material properties or section moment of area.

Keywords: CFRP, Field Hockey, CoDA Modelling, Composite Manufacture Techniques.

Contents

Abstract **2**

Nomenclature 5

1 Introduction **6**
1.1 History of the game **6**
1.2 Equipment function and FIH rules **9**
1.2.1 The stick 9
1.2.2 The ball 11
1.3 Composite materials **12**
1.3.1 Polymer matrix composites 12
1.3.2 Modulus of unidirectional composites and laminates 12
1.4 Modification of stiffness **14**
1.5 Aims and Objectives **19**

2 Modelling of shaft behaviour **20**
2.1 Introduction **20**
2.2 Methodology **20**
2.3 Results and discussion **24**

3 Preliminary Panel analysis **26**
3.1 Methodology **26**
3.1.1 Quasi-static flexure 26
3.1.2 Optical analysis 27
3.2 Results and Discussion **28**
3.2.1 Quasi-static flexure 28
3.2.2 Optical analysis 28

4 Control shafts **32**
4.1 Methodology **32**
4.1.1 Manufacture 33
4.1.2 Dimensions 33
4.1.3 Optical analysis 34
4.1.4 Quasi-static shaft flexure 34
4.2 Results and Discussion **35**
4.2.1 Dimensions 35
4.2.2 Optical analysis 36
4.2.3 Quasi-static shaft flexure 37

5 Multiple section shafts **38**
5.1 Methodology **38**
5.1.1 Manufacture 38
5.1.2 Hot pressing 39
5.1.3 Dimensions 40
5.1.4 Quasi-static shaft flexure 41
5.1.5 Dynamic drop-ball shaft flexure 42
5.1.6 Strain distribution 44
5.1.7 Optical analysis 45
5.2 Results and Discussion **46**

5.2.1 Dimensions 46
5.2.2 Quasi-static shaft flexure 48
5.2.3 Dynamic drop-ball shaft flexure 54
5.2.4 Strain distribution 56
5.3 Optical analysis 62
6 Conclusions 71
7 References 72

Nomenclature

FIH	Federation Internationale d'Hockey
I	Second moment of area
PMC	Polymer matrix composites
CFRP	Carbon fibre reinforced polymer
GFRP	Glass fibre reinforced polymer
EI	Flexural rigidity
UD	Uni-directional
E_{11}	The elastic modulus in the '1' or longitudinal direction
E_{22}	The elastic modulus in the '2' or transverse direction
G_{12}	The shear modulus in the 1-2 axes
ν_{12}	The 'major' Poisson's ratio
ν_{21}	The 'minor' Poisson's ratio
CoDA	Component design analysis
F	Force
L	Length
δ	Deflection
M	Moment
Q	Stiffness
a	Acceleration
v	Final velocity at maximum deflection i.e. Rest
u	Impact velocity
t	Time from impact to maximum deflection
M	Mass of hockey ball
CoR	Coefficient of restitution
f_1	Mode 1 bending frequency
C_1	3.52
m_0	ρ / A
ρ	Density
A	Section area

1 Introduction

1.1 History of the game

Evidence of a game similar to hockey has been found in tomb drawings in the Nile valley Egypt, dating back to 4,000 years ago. It then appeared again, during the middle ages throughout Europe, having various names like camocke (England) or shinty (Scotland). The modern game of hockey was however, developed in the public schools of England during the early 19th century. It then spread across Middlesex cricket clubs, such as Teddington, as a winter training exercise; much preferred to football. The game was played with an old cricket ball, using wooden sticks on the smooth cricket outfield. Basic rules including restriction of the backswing to lower than shoulder height and only being able to score inside a semi-circle in front of the goal, known as the "D" were introduced and in 1886 the Hockey Association was formed. The growth of hockey throughout the United Kingdom was rather sporadic as clubs from different regions often did not agree on rules. The introduction of hockey all over the British Empire during the late 19th century led to the first international competition between Ireland and Wales in 1895, the same year in which the International Rules Board was founded. Hockey first appeared in the Olympic Games in 1908 and became a permanent fixture in the Amsterdam games of 1928. By this time European countries played under a single structure or governing body known as the FIH (*Fédération Internationale d'Hockey*); the FIH is now a worldwide body, having 112 member states.

A major development in the game came with introduction of 'synthetic turf' in the 1970s; this led to a rapid increase in the speed at which the game was played and, to some extent, a loss of some skills, such as vertical stick stopping due to the predictability of the playing surface. The change in playing surface also led to a significant change in the design of the equipment, tactics and techniques used during play.

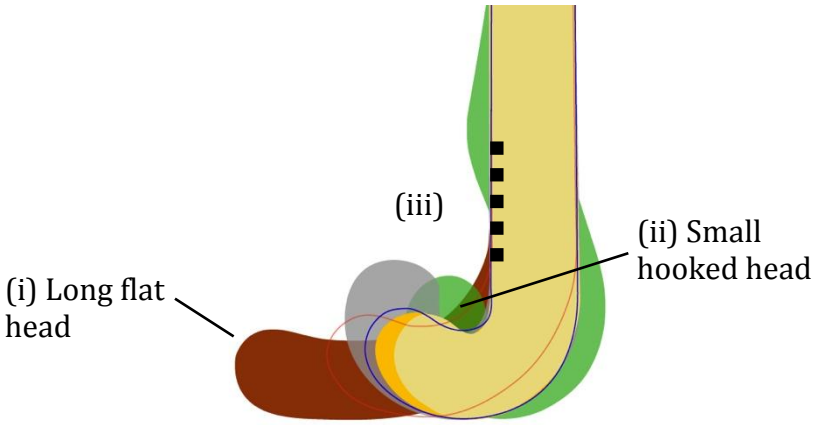

Figure 2.1 – The change of stick head shape as the game has developed. Progressively changing from the long flat head (i) to a smaller hooked shape (ii) and (iii) back-hand blade striking area.

The long head of the sticks were now not required, as the game became more accurate, only a small head, similar to the size of the ball, with a sharp hook on it began to be used (Figure 2.1). This allowed new skills such as the 'Indian dribble' and powerful back-hand blade striking shots to be performed. The Indian dribble skill was developed to allow the player to move the ball both left and right whilst moving forwards. The small hooked head could now be flipped over and used to achieve this. The back-hand blade shot is conducted with the head in this flipped over position and the ball is struck with the edge of the lower section of the shaft. The shot is more powerful due to the orientation of the stick; a simple look at the cross section of the two orientations (Figure 2.2) and the consideration of the second moment of area (found by $I = bh^3/12$), it can be seen that blade orientation has a higher second moment of area and therefore a theoretical higher bending stiffness.

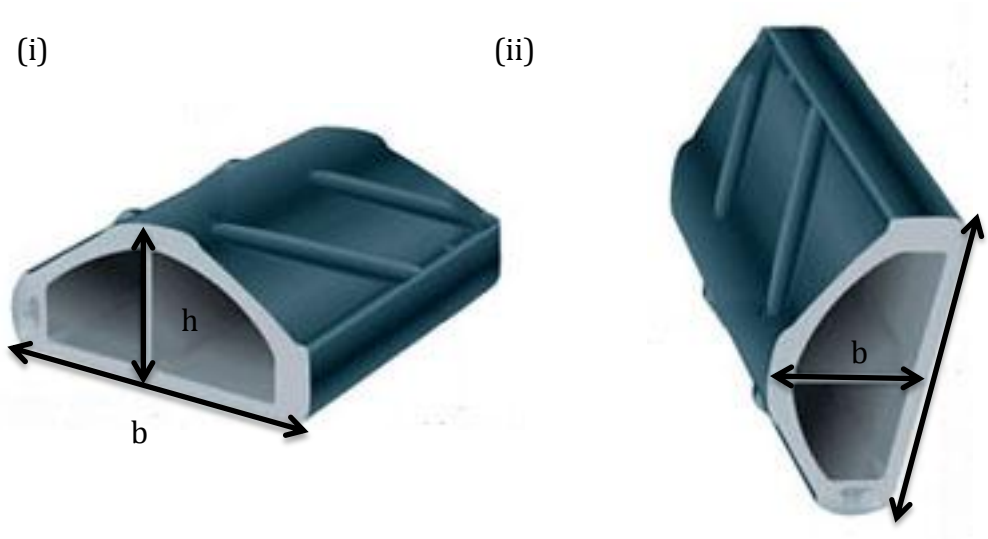

Figure 2.2 – Hockey stick cross sections in the (i) normal and (ii) blade orientations.

The construction of both the sticks and balls was developed in order to keep up with the new pace of the game. Sticks, originally made of mulberry now started to be made from composite materials, such as glass; carbon; and kevlar continuous fibre reinforced polymers and areas of discontinuous fibre reinforcements. The extra stiffness that the use of these materials gave the sticks was suited to a faster, more powerful game, however many players still prefer the 'feel' or 'comfort' they gain from the more compliant wooden sticks, allowing them to stop and control the ball more easily (McHutchon *et al.,* 2004). The old cricket balls became unsuitable for the water-based synthetic pitches as water absorption contributes to swelling of the cork core and creates a non-spherical cross-section, leading to inconsistent rolling behaviour. Hockey balls are now an example of solid ball construction being composed of mixtures of cork, wool and elastomer with a polyurethane (PU) or polyvinyl chloride (PVC) cover (Ranga *et al.,* 2008). The PU/PVC cover creates a seal around the water absorbing core materials and prevents the swelling and asymmetry found in cricket balls. The dimpled polymer cover, without the seam of leather cricket balls improved roll due to the completely spherical shape and aerodynamic consistency due to the stabilising affect the laminar flow around the ball created by the dimples, by delaying the occurrence of the separation of the flow, creating a smaller wake and therefore significantly less drag (Beasley and Camp, 2002).

Since its foundation in 1924 the FIH has been constantly reviewing and updating the regulations of the game. The premise of the game is now that two teams of eleven have to

negotiate a small polymer, cork and elastomer composite layered ball into a goal, using only the flat side of the sharply hooked stick during two halves of 35 minutes duration.

1.2 Equipment function and FIH rules

The constant review and updating of the rules of hockey by the FIH takes into account developments in surface and equipment technology; the nature of the current game; and, of course, the safety of participants. The following regulations, which focus on the rules regarding the stick and ball are taken from the field and equipment chapter of the Rules of Hockey, sections two and three respectively, published by the FIH, effective from 1st May 2009.

1.2.1 The stick

The hockey stick is used to impact and control the ball and so needs to transfer kinetic energy over a range of stick head speeds with good directional accuracy. The stick consists of four distinct sections, the handle (i), a taper (ii) to the blade section (iii) and the sharply hooked head (iv), (Figure 2.3).

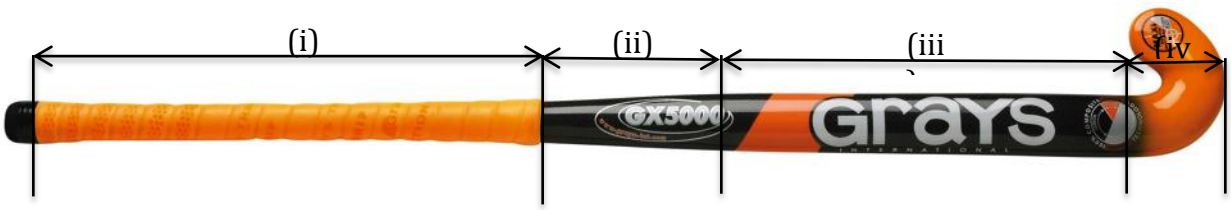

Figure 2.3 – Four distinct sections of the modern hockey stick. (i) The handle, (ii) taper from handle to blade, (iii) blade section and (iv) the sharply hooked head.

Variables contributing to how a hockey stick feels and performs include the mass, centre of mass location, shaft stiffness and resistance to twisting. The difficulty comes in achieving a design that can satisfy the variety of skills used during a game and the preference and ability of each individual player. In a study on perceived stick performance by McHutchon *et al.,* (2004) they found that for a hockey hit, all but one player chose a composite stick as their favourite, 18 out of 26 players chose the least stiff stick as their least favourite and 7

of them also chose the heaviest stick as their least favourite. They found that players were not able to interpret the correlation between perceived stick power and measured flexural rigidity (3-point bend, 0.8 m span over the blade section of the stick), but stiffer sticks were shown to be more powerful. The clamping conditions for both the laboratory and field-testing were however, different. In a field hockey hit the stick is held with both hands together at the end of the handle, making the full length of the stick under cantilever loading during impact. This is inherently different to the way the flexural rigidity was calculated, under different loading conditions and not taking into account the full span of the stick. There is therefore, no consideration on which section of the stick dominates the bending behaviour and how the change in the second moment of area of each section has an impact on this. The hit is also not a very good indicator of perceived control of the stick during stopping and dribbling skills as the stick is not put under as much loading and requires a finer adjustment to technique. When they considered dribbling skills, moment about the handle, centre of mass, or "pick-up weight" was found to be the most significant physical parameter and, in fact, the stick with the lowest stiffness, which was a wooden stick, was preferred by half the participants. This indicates a tradeoff between power and control of sticks and creates a large range of sticks of composite wrapped wooden sticks and full composite designs. With both high stiffness composite sticks intended for pure power and less stiff wooden sticks designed purely for control. Most of the market is however directed at trying to create a stick that satisfies both these parameters in varying degrees.

Stick manufacturers classify their sticks in two main ways. The mass of the stick, being super light, light, medium or heavy and in the power of the stick. Both of which are not truly comparable quantitatively within or between manufacturers. In McHutchon *et al.,* (2006) all tested sticks, all from the same manufacture, were graded as a having a medium mass, however physical mass ranged between 0.565 kg and 0.618 kg. The power rating ranged from medium to extra stiff, with no actual measured stiffness values associated with this. Most of the design parameters are left down to the manufacturer; however the FIH sets out the following rules and regulations.

Materials:

a The stick and possible additions may be made of or contain any material other than metal or metallic components, provided it is fit for the purpose of playing hockey and is not hazardous.

b The application of tapes and resins is permitted provided that the stick surface remains smooth and that it conforms to the stick specifications.

1.2.2 The ball

There is only one ball that meets the FIH specifications (FIH, 2009) for international matches, the Kookaburra HB 410 Elite MK II. It has a complex construction consisting of an elastomer core with a wool-bound outer resin-bonded cork layer and a PVC cover. Other non-conforming balls used in non-international matches are constructed of a layered cork core with a PU or PVC cover, as shown in Figure 2.4.

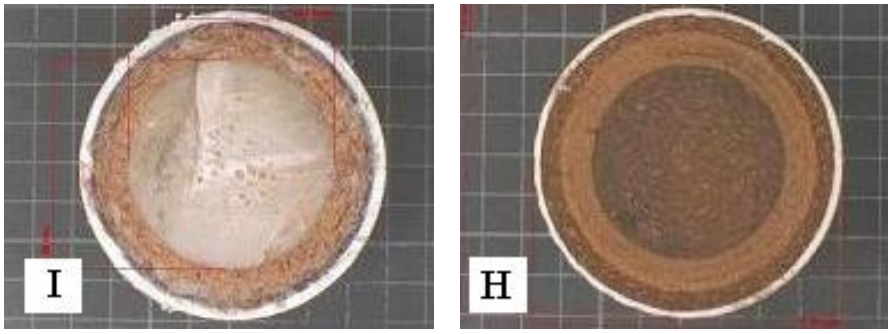

Figure 2.4 - Cross-sectional images of (I) elastomer cored FIH conforming ball and (H) layered cork cored non-conforming ball (Ranga *et al*., 2008).

When the ball is stationary and is impacted by the stick travelling at speed, the behaviour of the ball and stick is as follows. During the collision between the ball and the stick two phases occur in the contact period, compression and then a restitution phase. The point at which this phase change occurs is when the normal relative velocity of the ball centre of mass and the stick centre of mass becomes zero. Both the stick and ball are allowed to travel in the same plane, so when the stick impacts the ball, the ball begins to compress and the stick deflects. The stick and ball travel as one body whilst this compression continues, until the velocity of the ball (which is increasing) and the velocity of the stick (which is decreasing) become equal. The stored strain energy in the ball is then released to propel the ball away from the stick. The contribution of the strain energy stored in the stick as it deflects is unknown, as is how the stiffness of the stick affects this. With a combination of the release of strain energy from both bodies during impact the resulting ball speed could

theoretically be higher, as the release in strain energy from the ball and stick covert into kinetic energy transferred to the ball.

1.3 Composite materials

1.3.1 Polymer matrix composites

The majority of polymer matrix composites (PMCs) used in sport consist of a high modulus or high strength fibre (glass, carbon or Kevlar) in resin (epoxy or phenolic) matrix, the most commonly used being carbon fibre reinforced polymer (CFRP). The resin matrices cross-link during curing, which involves the application of heat and pressure via an autoclave, hot press or vacuum bag. Variation in fibre and resin type along with orientation and volume fraction are used to control modulus and strength properties along with anisotropy.

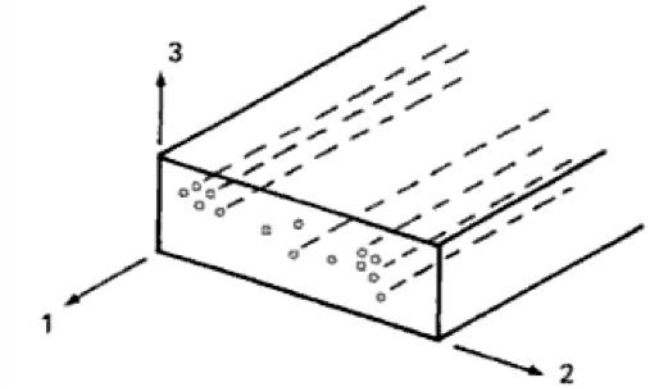

Figure 2.5– Orientation of principal material axes (Mathews and Rawlings, 1994).

1.3.2 Modulus of unidirectional composites and laminates

Considering a composite in which all fibres are aligned in one direction (unidirectional or UD composite), the properties of this basic form of a composite can then be used to predict the behaviour of more complex multi-directional laminates. The properties along the fibre length (1) direction are very different from those in the other two directions (2, 3). Such a material is known as 'orthotropic'. The elastic properties are symmetric with respect to the principal material (1-2-3) axes (Figure 2.5).

The basic stress-strain relations for UD composites are the same as those for an isotropic material, although the constants are direction-dependent. When the directions of the

applied stresses coincide with the principal (1-2) material axes, strains in terms of stress are as follows:

$$\varepsilon_1 = \frac{\sigma_1}{E_{11}} - \nu_{21}\frac{\sigma_2}{E_{22}}$$

$$\varepsilon_2 = -\nu_{12}\frac{\sigma_1}{E_{11}} + \frac{\sigma_2}{E_{22}}$$

$$\gamma_{12} = \frac{\tau_{12}}{G_{12}}$$

where:

E_{11} = the elastic modulus in the '1' or longitudinal direction,

E_{22} = the elastic modulus in the '2' or transverse direction,

G_{12} = the shear modulus in the 1-2 axes,

ν_{12} = the 'major' Poisson's ratio, and

ν_{21} = the 'minor' Poisson's ratio.

In practical applications, CFRP is not used in single plies and is often not stressed solely along the longitudinal axis. UD plies are usually stacked in a variety of orientations and thicknesses to form laminates with the required modulus and strength properties. This often results in plies where the fibres are no longer aligned parallel to the applied stresses; these are rotated layers and are subjected to off-axis loading. A number of laminate theories (Matthews and Rawlings, 1999; Tsai and Hahn, 1980) have been developed to estimate mechanical properties based on individual ply orientations and properties.

Established convention for denoting both the lay-up and stacking sequence of a laminate is as follows. For example, a 4-ply laminate, which has the fibre orientation in the sequence 0°, 90°, 90°, 0° from the upper to the lower surface would be shown as $(0/90)_s$. The suffix 's' means that the stacking sequence is symmetric about the mid-thickness of the laminate. To clarify the laminates $(0/45/90)_s$ and $(45/90/0)_s$ have the same lay-up, but a different stacking sequence.

The in-plane modulus of a laminated composite can be obtained directly by applying the rule of mixtures equation to the modulus of the unidirectional composite and is simply the arithmetic average of the modulus of the constituent plies. All the information that is required is the orientation and the volume fraction of each ply group; this will not apply to off-axis ply containing laminates howe

1.4 Modification of stiffness

Investigation into the stiffness of composite sticks, bats and shafts has been carried out for a number of years relating to various sports (Smith, 2001; Pearsall *et al.,* 1999; Cheong *et al.,* 2006), in particular for golf shafts (Butler and Winfield, 1994).

The stiffness of a shaft can in theory exert a significant influence on resulting ball velocity. When an elastic material such as CFRP is deformed, potential energy is stored in the material in the form of strain energy. This strain energy can then be converted to kinetic energy at impact, leading to a greater impact speed and hence resultant ball speed. The ability of the shaft to store and release this energy depends greatly on shaft stiffness. Optimisation of impact speed in golf drivers, to achieve maximum drive distance and in field and ice hockey to attain high resultant shot speeds is greatly desired (Van Gheluwe *et al*., 1990). The capability of the shaft to maximise this depends on the conversion of strain energy into kinetic energy and therefore shaft behaviour is optimised by shaft stiffness. However the mechanics of the impact also affect whether shaft stiffness must be maximised or more specifically tailored to achieve this.

The stiffness variation along the length of golf shafts and the cause of this variation was addressed by Huntley (2006) using static and dynamic stiffness analysis over a range of golf shafts and relating this to microstructural characterisation. The flexural rigidity distribution was determined using Broulliette's interpretation of the Euler-Bernoulli slender beam equation (Broulliette, 2002). The method involved a mass being hung from the tip, the deflection was then measured for the shaft clamped at progressively larger distances from the tip. This produces a stiffness profile for the entire length of the shaft. This study identified the importance of the stiffness distribution on shafts by documenting three shafts of similar end deflection, yet widely different flexural rigidity profiles. The flex, or kick point in golf shafts, which is controlled by the degree of taper and the lay-up of the CFRP, is the point at which maximum deflection occurs and influences the release of the head into the ball at impact and hence power, trajectory and accuracy. The head of the golf club can be considered to bend around three orthogonal axes about the butt or grip end of the shaft, prior to impact. The y-axis is from the back to the face of the clubhead, the x-axis is from the heel to the toe and some twisting about the longitudinal z-axis can also occur (Figure 2.6). Deflection about the y-

axis occurs in both the lead (positive deflection about neutral z axis) and lag (negative direction about neutral z axis) directions, whereas deflections about the x-axis occur in toe-up or toe-down directions about the neutral axis. The degree of deflection in the y-axis is the only deflection that contributes to clubhead speed, and although deflections about the x-axis cannot contribute to speed it can have an effect on the trajectory and accuracy of the ball flight (Figure 2.7).

The flexural rigidity distribution along the shaft therefore has a key role in controlling

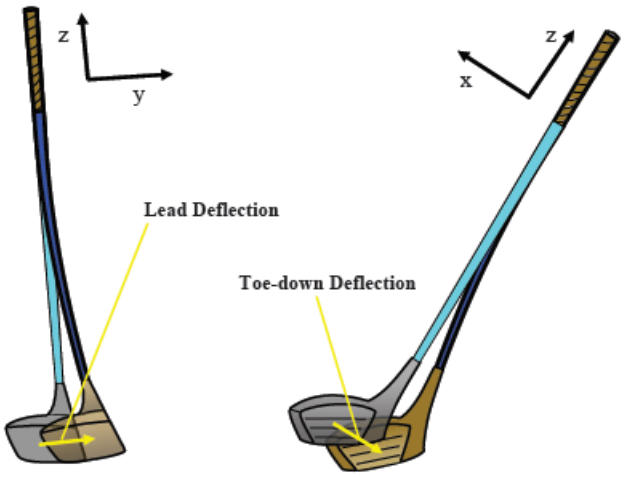

Figure 2.6 – Shaft deflection about three orthogonal axes prior to impact (MacKenzie, 2005)

the golf shaft's performance, and so by varying this stiffness along the shaft, different shaft behaviour can be achieved.

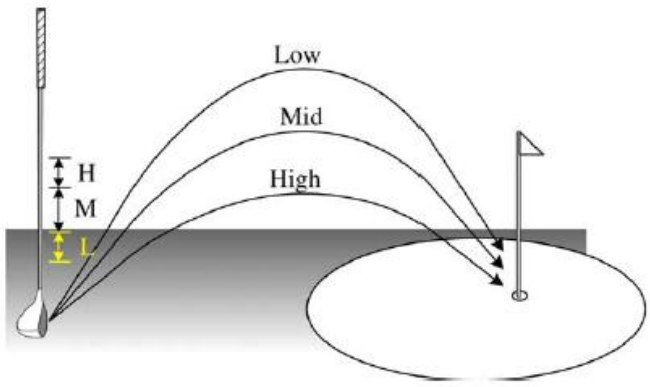

Figure 2.7 – Effect of "kick-point" location on ball flight trajectory (Cheong *et al.*, 2006)

A similar study by Cheong *et al.,* (2006) successfully used finite element modelling (FEM) to predict the performance of golf shafts with respect to their construction and found a good correlation between experimental results and the FEM with no greater

Table 2.1 – Comparison between experimental and FEM numerical data (Cheong *et al.*, 2006)

	Numerical data	Experimental data	Error (%)
Deflection (mm)	375.0	367	2.2
Torsional angle (deg.)	4.1	4.2	2.4
Frequency (Hz, CPM)	4.1, 244.2	250.0	2.3
Kick point (mm, %)	450.5, 38.5	460.0, 38.3	2.1
Weight (g)	53.2	52.4	1.5

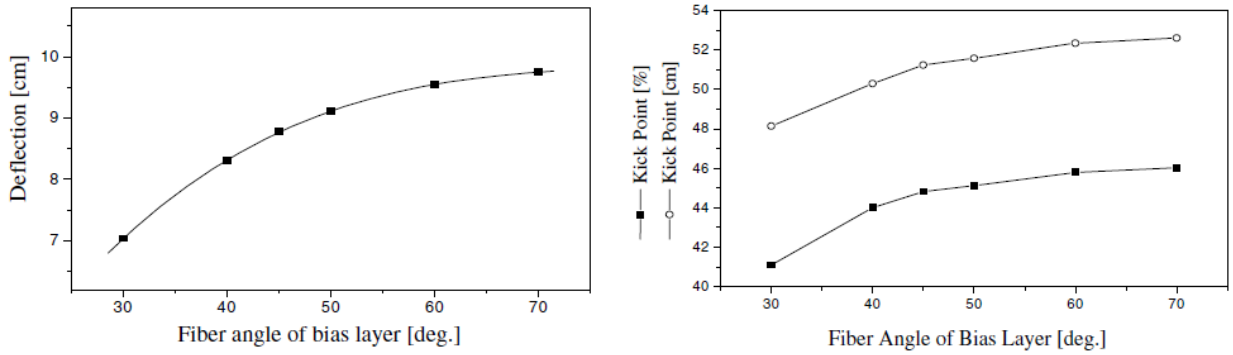

Figure 2.8 – Effect of fibre orientation on deflection and kick point location (Cheong *et al.*, 2006)

than a 2.4 % error (Table 2.1). The numerical results also showed that the major parameters of golf shafts are strongly dependent in terms of deflection and kick point location, on the material properties of the fibres and lay-up of the laminate, therefore the fibre orientation and the location of the kick point along the shaft (Figure 2.8).

The behaviour of other shafted sports equipment such as ice hockey sticks has been dealt with in a more rudimentary way. Stick stiffness has been considered as an overall entity by way of a 3-point bend test in four models of stick; medium (13 kN m^{-1}), stiff (16 kN m^{-1}), extra (17 kN m^{-1}) and pro stiff (19 kN m^{-1}) by Pearsall *et al.* (1999). They found that when subjects performed a slap-shot, puck velocity was highest for the stick with a stiffness of 13 kN m^{-1} (108.2 km h^{-1}) and lowest for the stick with stiffness of 17 kN m^{-1} (105.9 km h^{-1}). This suggests that lower stick stiffness is beneficial to achieve a higher puck velocity ($P < 0.05$), however it is also important to consider the subject influence in this study and the different mechanics involved in comparison to the golf swing or field hockey hit. The slap shot is held with both hands around 40 - 60 cm apart on the stick and involves six distinct phases; backswing, downswing, preloading, loading, release and follow through (Pearsall *et al.,* 1999). In the pre-loading phase the stick first makes contact with the ice and begins stick bending, the stick blade then impacts the puck and they travel together in the loading phase before the strain energy stored in the stick is released in the form of kinetic energy through the puck. The

mechanical factors important in the slap shot have been identified as (1) velocity of the lower (distal) end of the shaft prior to contact with the ice; (2) preloading of the stick; (3) elastic stiffness characteristics of the stick and (4) contact time with the puck (Doré & Roy 1976; Hoerner 1989).

The correlation between field hockey stick stiffness and ball speed was investigated in a similar way to Pearsall *et al.* (1999) by McHutchon *et al*. (2004). Three wooden sticks (EI - 308 Nm^2, mass - 0.59 kg; 556 Nm^2, mass – 0.66 kg and 460 Nm^2, mass – 0.62 kg) and one CFRP stick (EI – 1041 Nm^2, mass – 0.62 kg) were analysed initially by a 3-point bend test, then subjected to high speed video documented impacts by four experienced players. Focusing on sticks three (460 Nm^2, mass – 0.62 kg) and four (1041 Nm^2, mass – 0.62 kg) they showed that a 10 % increase in ball speed could be attributed to a 100 % increase in overall stick stiffness, the mass of these sticks was kept constant, however the centre of mass from the handle (0.556 m and 0.544 m) for sticks 3 and 4 respectively was not.

The mechanics of the field hockey shot are similar to that of the golf swing in that there are no pre-loading or loading phases. The stick impacts the ball, deflects as the ball deforms, storing strain energy in both bodies and they travel as one, before the stick and ball both release the stored energy and the ball accelerates away from the stick (Carlisle, 2009). The variation of this stiffness, the placement of the flex point or the relationship with the centre of mass of the sticks was not explored in order to try and explain this relationship. Much like golf shafts and ice hockey sticks, there is little comparability between manufacturer-claimed descriptions of field hockey stick stiffness; for this reason Covill *et al.* (2008) aimed to quantify the static stiffness behaviour of a variety of hockey sticks, and to move towards a standard for their characterisation. This was done by conducting 3-point bend tests at two spans each 228 mm wide along the sticks, A (173 mm from head to point of compression) and B (388 mm from head to point of compression). Variation in the construction between different models and manufacturing variations within models were noted as stated by the manufacturer. No scientific explanation was given for the estimated composition of the sticks and so the relationship of stick composition (% of CFRP, GFRP and Kevlar reinforcing fibres) to stick stiffness cannot be made. The composition is stated as a percentage, this however does not allow for the variation in composition along the length and its contribution to stick stiffness, along with the second moment of area. The

main findings of the study however showed that in all of the sticks tested (9 models, 1 - 6 examples per model) the flexural rigidity closer to the handle (430 – 1069 Nm^2) was greater than in the blade section (310 – 636 Nm^2), and that in some cases there was significant deviation within models (Table 2.2).

Table 2.2 – Variety, mass composition and flexural rigidity of sticks used in Covill *et al.* (2008).

Stick number	Mass (g)	Estimated composition			Mean flexural rigidity closer to the handle (B) (Nm^2)	Mean flexural rigidity closer to the blade (A) (Nm^2)
		Carbon %	Aramid %	Fibreglass %		
1	603 ± 14	20	20	60	310 ± 13	430 ± 21
2	602 ± 13	30	20	50	329 ± 23	631 ± 35
3	605 ± 33	90	10	-	453 ±19	567 ± 24
4	567 ± 12	35	15	50	410 ± 28	451 ± 65
5	581	85	15	-	505	1069
6	576	85	15	-	387	607
7	564 ± 24	50	5	45	471 ± 28	730 ± 75
8	609 ± 15	50	15	35	552 ± 23	646 ± 29
9	583 ± 9	100	-	-	636 ± 30	742 ± 38

The construction of a robot capable of swinging hockey sticks at an impact speed of up to the maximum recorded in-game speed of 46.03 ± 11.58 ms^{-1} (Rai *et al.,* 2002) by Carlisle (2009) to investigate the interaction between stick and ball at impact and the applicability of FIH testing procedures on hockey balls to match scenarios, has the potential to conduct comprehensive stick testing. This would allow a true analysis firstly of the variation in static stiffness along the length of a stick using Broulliette's equations, how this relates to stick performance and then to the microstructure and construction of the sticks.

1.5 Aims and Objectives

- Model the behaviour of carbon fibre shafts, with multiple sections along the shaft of varied fibre orientation to investigate how this affects overall stiffness behaviour of the shaft.
- Manufacture a selection of shafts that represent the overall stiffness of current hockey stick market found by Covill *et al* (2008), using hand lay-up and hot pressing techniques.
- Test the shafts under static and dynamic loading conditions and assess their behaviour in relation to the modelled predictions and behaviour highlighted by Pearsall et al. (1999) by McHutchon et al. (2004).
- Assess the hand lay-up and hot-pressing techniques for volume fraction, ply-orientation and interaction of varied lay-up sections.

2 Modelling of shaft behaviour

2.1 Introduction

In order to produce shafts with the relevant flexural rigidity in comparison to existing sticks and to understand how to manipulate the lay-up in order to create "kick points" in the shaft, classic laminate theory was applied to parallel sided shafts. This involved using CoDA (Component Design Analysis) software and an adapted version of Brouilette's equation, resulting in a database of different lay-up, and weak point location effect on the overall flexural rigidity of composite shafts. From these lay-ups were selected for fabrication using hot pressing for more detailed analysis.

2.2 Methodology

Technical data of MTM28/High Strength-T700 carbon fibre uni-directional pre-preg sourced from Advanced Composites Group Ltd. were input into the CoDA software. The essential mechanical properties are detailed in table 3.1**.**

Table 3.1 – Mechanical properties of MTM28 /Carbon UD Prepreg

Property	**Value**
Density (kgm^{-3})	1480
E_{11} (GPa)	97.46
E_{22} (GPa)	4.3
G_{12} (GPa)	8
G_{13} (GPa)	8
ν_{12}	0.3

The mechanical properties of the UD prepreg were input into the software to create plies of the desired properties and orientations so that elastic modulus and moment of inertia data for different laminates and section dimensions could be predicted. The CoDA software is limited to applying these data to homogenous laminate beams, and cannot therefore predict the flexural rigidity of beams with two or more sections of

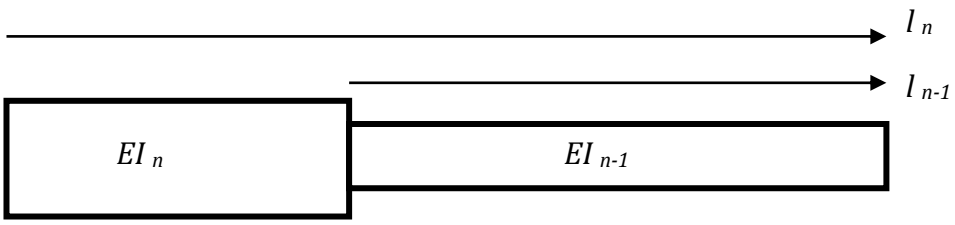

different lay-ups along its length. To do this Brouilette's equation (1) for calculating the flexural rigidity of progressively larger sections of cantilever loaded beams was manipulated so that it predicted the deflection of known flexural rigidity sections (2); the stiffness (Q) of the entire shaft made up of different sections can be then be found and therefore the overall flexural rigidity could be calculated (3)(4).

Where - EI = Flexural rigidity (Nm^2)

F = Force (N)

L = Length (m)

δ = Deflection (m)

M = Moment (Nm)

Q = Stiffness (Nm^{-1})

and

$$EI_n = \frac{\frac{1}{3} F\,(l_n^3 - l_{n-1}^3)}{\delta(l_n) - \frac{1}{3}\left(\frac{M_{n-1} l_{n-1}^2}{EI_{n-1}}\right)}$$

(1)

$$\delta(l_n) = \frac{F\,(l_n^3 - l_{n-1}^3)}{3\;EI_n} + M_{n-1}\left(\frac{l_{n-1}^2}{3\;EI_{n-1}}\right)$$

(2)

$$Q_{shaft} = \frac{F}{\delta}$$

(3)

$$EI_{shaft} = Q\,x\,\frac{l_n^3}{3}$$

(4)

This method was applied to 0.5 m long shafts with a second moment of area (I) of 6.59 $x10^{-9}$ m^4 (radius 0.0125 m and wall thickness 0.00125 m, or 10 plies). The dimensions were chosen to maintain the resultant EI values within the boundaries of previously characterised hockey sticks by McHutchon *et al.* (2006) of between 389 Nm^2 and 708 Nm^2 and to keep the wall thickness low. The following lay-ups and corresponding flexural rigidity (Table 3.2) were input equations 1 and 2 in various permutations. The shaft was theoretically split up into five and ten sections and a combination of a stiffer lay-up and a weaker lay-up were chosen. The weak lay-up would be positioned increasingly further away from the clamped end of the shaft in 0.05 m or 0.1 m increments to assess the effect this had on overall flexural rigidity of the shaft (Figure 3.1). The combination of weak sections and normal sections was chosen so that the weak point had either a 15 or 30% lower flexural rigidity. The combinations initially experimented with are shown in table 3.3.

Table 3.2 - Modulus, second moment of area and flexural rigidity data for various laminates.

10 PLY r = 12.5 mm			
Lay up	**E (GPa)**	**I (x $10^{-9}m^4$)**	**EI Nm^{-2}**
0/45/-45/45/-45 s	39	6.59	257.01
0/90/90/90/90 s	42.2	6.59	278.2825
90/0 s	54.4	6.59	358.529
0/45/90 s	55	6.59	362.6543
0/30/-30/30/-30 s	56.7	6.59	373.653
0/45 s	65.4	6.59	431.2826
0/90 s	66.5	6.59	438.2021
0/20/-20/20/-20 s	73.3	6.59	483.047
0/10/-10/10/-10 s	85.6	6.59	564.104
0	90	6.59	593.1

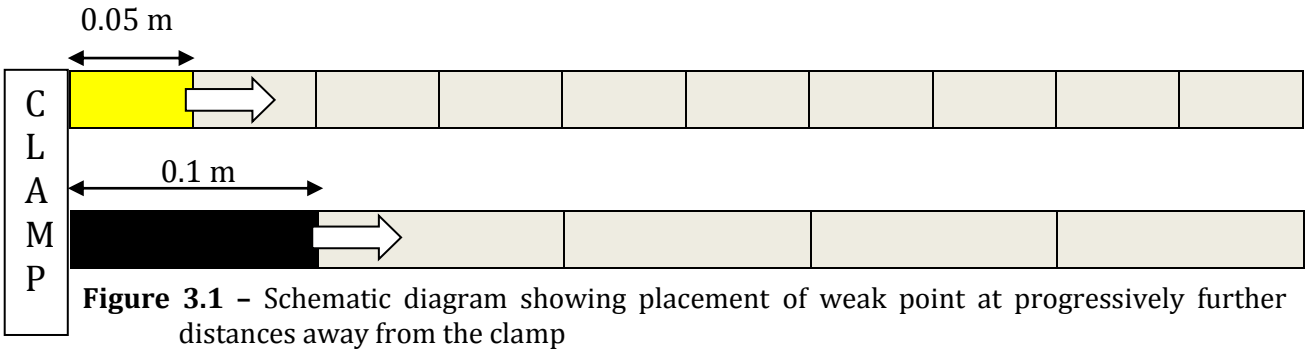

Figure 3.1 – Schematic diagram showing placement of weak point at progressively further distances away from the clamp

Table 3.3 - Combinations of weak point and normal section lay-ups initially chosen

0.1 m/ 0.05 m increments	Lay-up	Flexural rigidity (Nm^2)	Flexural rigidity decrease (%)
	0/45 s	431.28	
	0/45/90 s	362.65	15.91
	0	593.1	
	0/45 s	431.28	27.31
	0/45 s	431.28	
	0/90/90/90/90 s	278.28	35.5
	0/20/-20/20/-20 s	483.04	
	0/10/-10/10/-10 s	564.1	14.4
	0/30/-30/30/-30 s	373.65	
	0/10/-10/10/-10 s	564.1	33.76

2.3 Results and discussion

A number of preliminary inputs into the model and a re-assessment of the ability to hand lay-up 90° fibres lead to a narrowing down of the lay-ups and increments that were suitable. Figure 3.2 shows a number of scenarios that indicate the degree or size of

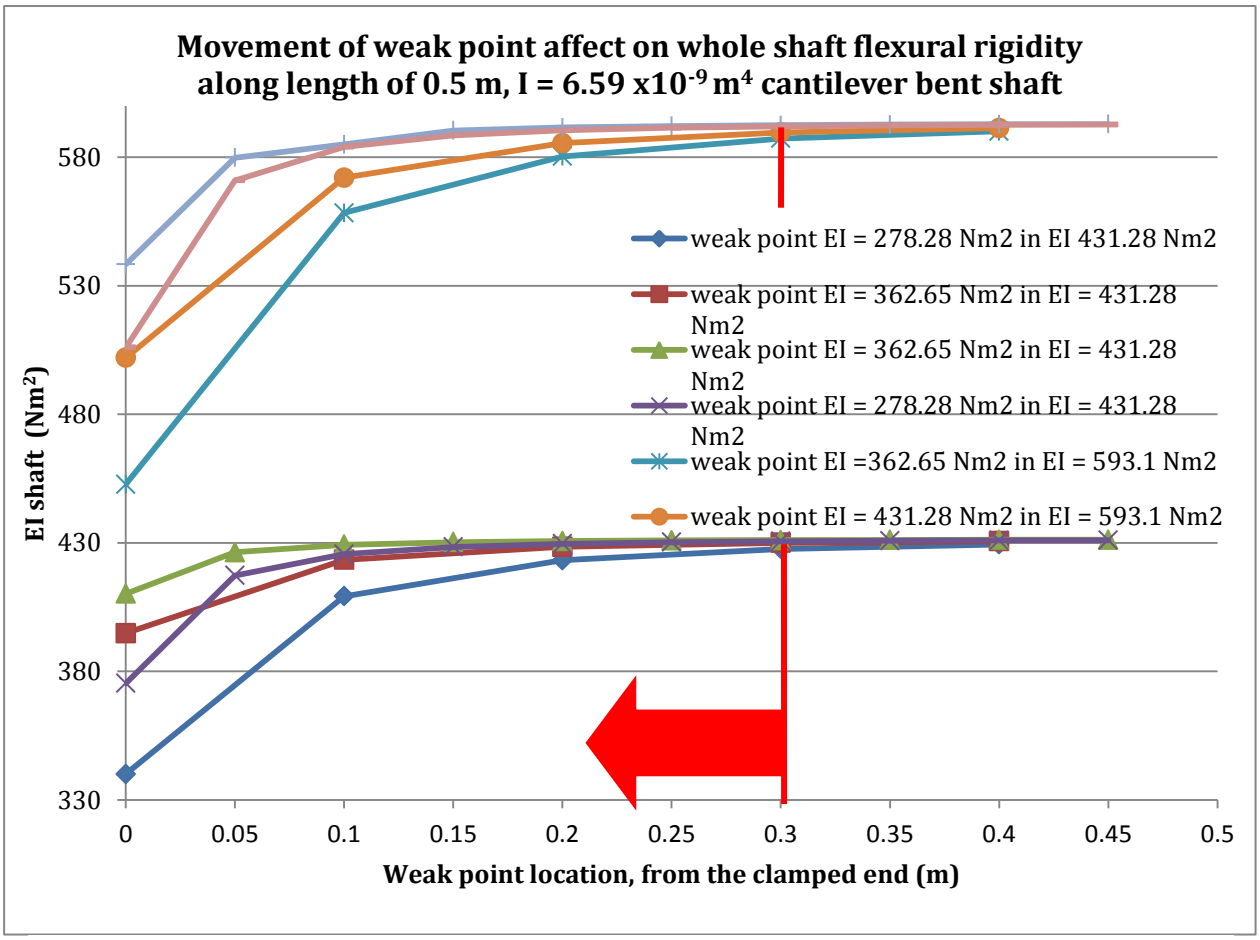

Figure 3.2 – Demonstration of the negligible effect of the weak point when it is over 0.3 m away from the clamped end of the shaft, regardless of the EI combination.

the weak point, it stops having an effect on overall flexural rigidity around 0.3 m away from the clamp. For this reason no further investigation into the position of the weak section past this point was conducted. The number of lay-ups that were considered feasible was narrowed down to those only containing fibres at an angle of less than 45°, due to the hand lay-up difficulties experienced with plies above this angle. The difficulty of preparing and laying-up sections of 0.05 m was also addressed and reviewed, and using weak sections of 0.1 m was chosen to be more practical.

As previously stated the overall stick flexural rigidity data produced by McHutcheon (2006) for a range of Gray's sticks identified a range between 389 and 708 (Nm^2). The upper end of this is difficult to produce with the dimension restraints for the shafts, however ignoring the upper end stick in McHutcheon's tests the range is narrowed to 389 - 557 (Nm^2), which can certainly be replicated. Using the $(0/10/-10/10/-10)_s$ laminate as the base matrix for the shaft and then using 0.1 m weak sections of both $(0/20/-20/20/-20)_s$ and $(0/30/-30/30/-30)_s$ a range of overall shaft flexural rigidity of 340 – 561.8 (Nm^2) can be produced. This is shown in Figure 3.3.

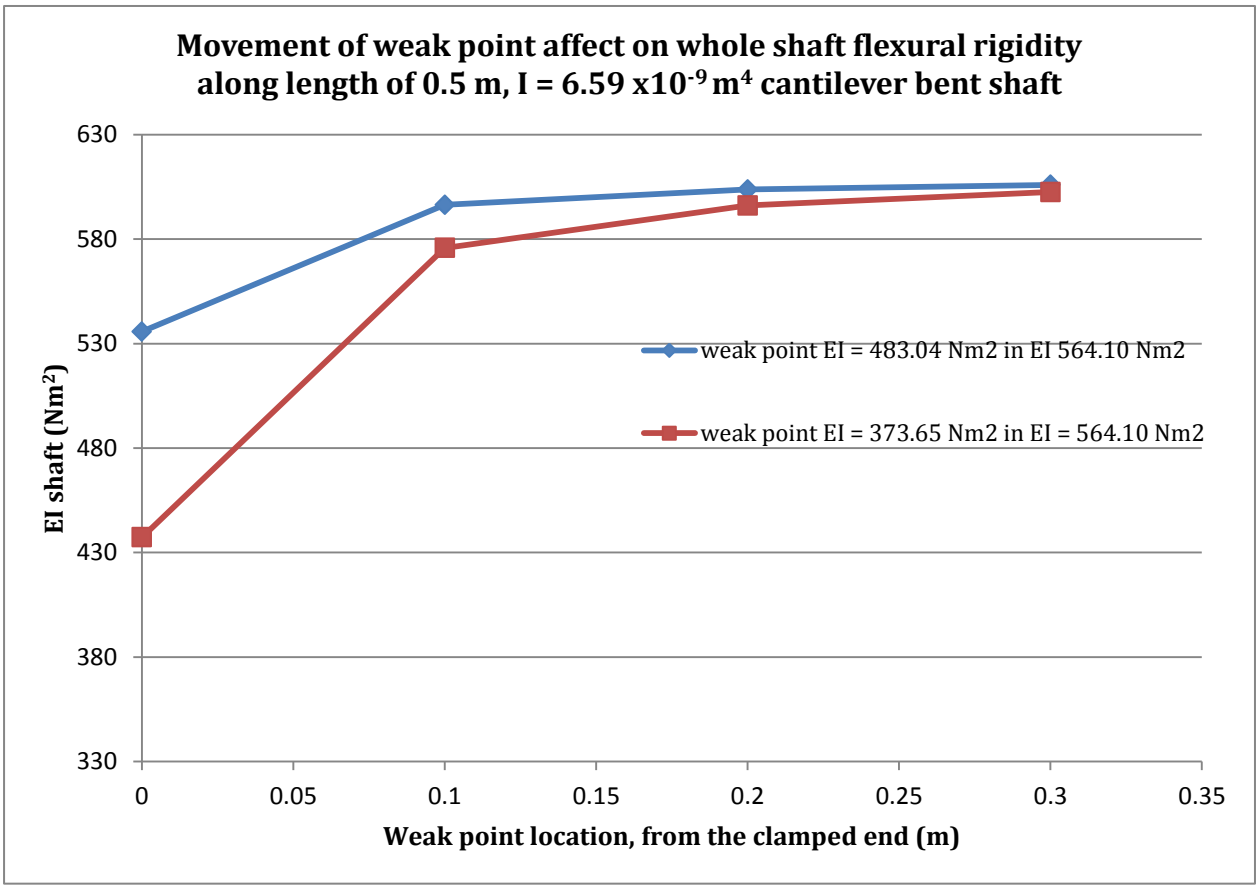

Figure 3.3 - $(0/10/-10/10/-10)_s$ laminate as the base matrix for the shaft and 0.1 m weak sections of both $(0/20/-20/20/-20)_s$ and $(0/30/-30/30/-30)_s$.

Manipulating these two combinations would produce eight beams with flexural rigidity of 340.04, 409.23, 423.21, 427.64, 451.74, 530.31, 553.64 and 561.8 Nm^2 respectively, to be fabricated by hot pressing for detailed analysis.

3 Preliminary Panel analysis

3.1 Methodology

Three 10 ply panels were fabricated, with sections of different lay-ups, detailed in figure 4.1, using ACG MTM28/T800 unidirectional (UD) pre-preg. with a stated fibre volume fraction of 0.55. The panels were vacuum bagged and cured in an oven using a three stage thermal cycle; temperature was ramped up to 125 ˚C at 0.5 ˚C min^{-1}, held for 1 hour and then cooled at 3 ˚C min^{-1}. The panels were then measured using digital callipers (Mitutoyo Absolute Digimatic), taking ten readings of width, length and depth respectively.

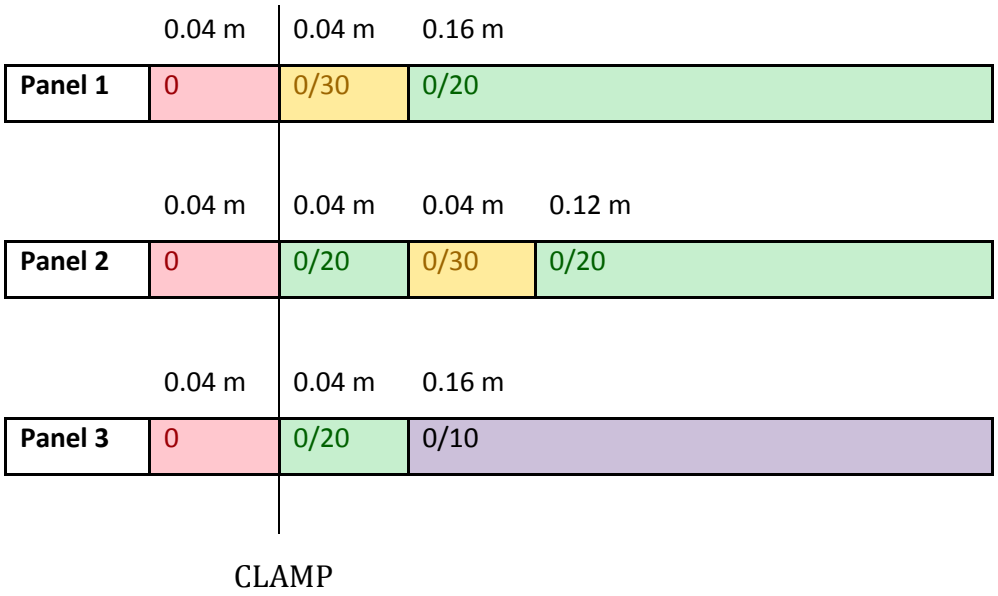

Figure 4.1 – Lay-up configurations of three varied lay-up panels, showing initial clamping location and control section (0°) in red.

3.1.1 Quasi-static flexure

The panels were clamped in the 0.04 m control section, (shown in red in figure 4.1), and the tip deflected by 11 mm over a cantilever length of 0.2 m, at a rate of 10 mm/min, before returning to zero deflection. There was a pre-load of 2 N to ensure full load-point / sample contact. Loading was carried out in an Instron 3345 test frame with a 5 kN load cell and Bluehill software (Figure 4 .2). The clamping was then moved to the 0.4 m 0/30, 0/30 and 0/20 in panels 1 (0.16 m cantilever length), 2 (0.12 m cantilever length), and 3 (0.16 m cantilever length) respectively in order to determine the modulus of the 0/20 and 0/10 sections. In these sections in the three panels, the cantilever

length was long enough to provide an accurate modulus value using $E = \frac{F\,l^3}{3\delta I}$ and $I = \frac{bh^3}{12}$.

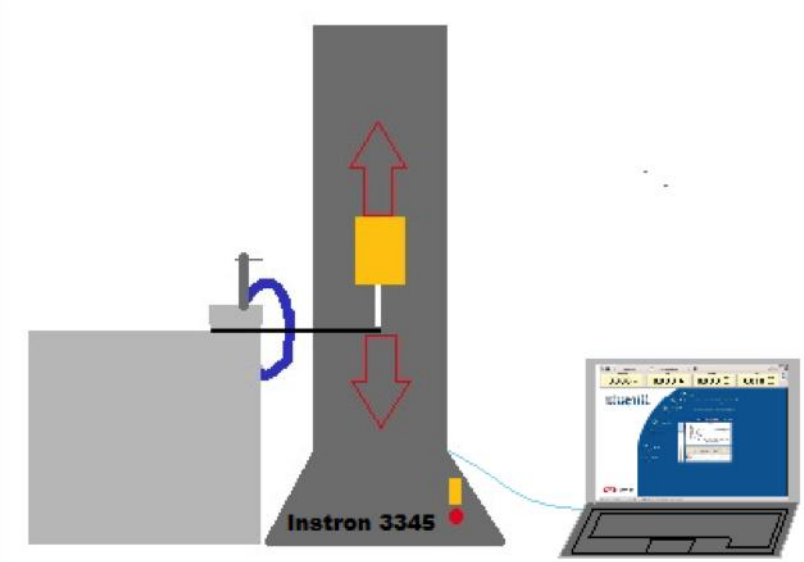

Figure 4.2 - Schematic diagram of the cantilever static panel flexure using the Instron 3345 and Bluehill software.

3.1.2 Optical analysis

Seven transverse cross-sections and four longitudinal cross-sections were obtained using a Buhler multi tool and a Struers Accutom, (16.7 mm x 10 mm). Transverse cross sections were taken from the seven different lay-up sections and the longitudinal cross-sections were taken from the seam at which they join. They were mounted in Durafix resin and polished to a 1 µm diamond paste finish. Samples were then inspected using Zeiss microscope and Image J analysis software. The panels were characterised for ply thickness, fibre volume fraction, ply orientation and seam cross-sectional area.

3.2 Results and Discussion

3.2.1 Quasi-static flexure

The varied lay-up panels showed a higher modulus than was predicted by the modelling equation. Panel 1 a 17.22 % increase, panel 2 a 16.13 % increase and panel 3 a 14.31 % increase over the prediction (Fig. 4.3). The presence of the seam between sections does

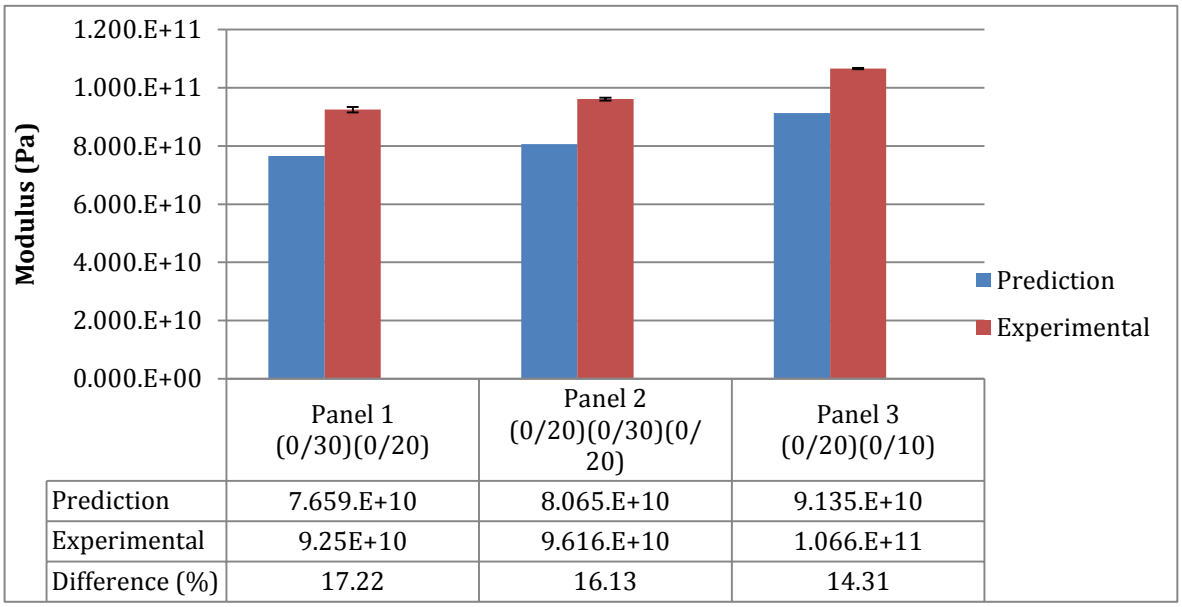

	Panel 1 (0/30)(0/20)	Panel 2 (0/20)(0/30)(0/20)	Panel 3 (0/20)(0/10)
Prediction	7.659.E+10	8.065.E+10	9.135.E+10
Experimental	9.25E+10	9.616.E+10	1.066.E+11
Difference (%)	17.22	16.13	14.31

Figure 4.3 – Comparison of experimental and predicted panel modulus values.

not; therefore reduce the overall modulus of the panel. The seam could affect the load transfer, as the matrix dominates the longitudinal behaviour in these sections. The presence however, of the continuous longitudinally orientated plies 1 and 10 is sufficient to transfer the applied load adequately. The resulting panel modulus would therefore have been reduced and brought the experimental and predicted moduli closer together.

3.2.2 Optical analysis

Having found a higher than predicted modulus in all three panels, an analysis of the fibre orientations through the different panel sections was conducted, as variation in the orientation of the fibres in the different sections could have had an effect. The average volume fraction for the panels was consistent (52.93 ± 0.3%), similar to that

produced in previous vacuum bagged panels. The orientation of the plies throughout the sections in all three panels was very close to the intended orientations (Table 4.1). The maximum average deviation from the intended orientation in all the sections was 1.67° in the panel 1 (0/20) section with an average deviation over all sections of 0.45°. This validates the reproducibility of the hand-layup process as the (0/20) section was repeated four times through the three panels.

Table 4.1 – Summary of the predicted and experimental moduli and lay-ups of the three panels studied.

	Panel 1 (0/30)(0/20)		**Panel 2 (0/20)(0/30)(0/20)**			**Panel 3 (0/20)(0/10)**	
Predicted Modulus (GPa)	76.6		80.6			91.4	
Experimental Modulus (GPa)	92.5		96.2			107	
Difference (%)	17.21		16.13			14.30	
Fibre volume fraction (%)	53.25		52.50			53.02	
Ply Orientation	**(0/30)**	**(0/20)**	**(0/20)**	**(0/30)**	**(0/20)**	**(0/20)**	**(0/10)**
1	0	0	0	0	0	0	0
2	28.71	22.09	18.6	26.66	22.15	19.8	11.15
3	28.12	21.53	20.03	27.46	22.53	21.03	9.23
4	29.08	21.13	19.15	31.89	20.13	20.15	9.56
5	31.46	23.17	18.39	31.42	22.17	19.39	10.54
6	31.12	19.11	19.11	28.57	20.16	20.22	11.73
7	31.16	22.78	19.15	31.2	22.78	20.22	9.24
8	30.55	20.57	20.81	30.55	21.27	21.61	9.91
9	31.33	22.99	20.4	31.21	21.99	20.47	8.53
10	0	0	0	0	0	0	0

The join between sections of different lay-up is expected to produce resin-rich regions, which could have an effect on overall modulus. The effect on static modulus up to 20 N load was, however difficult to see due to the stressing system and lay-up. The longitudinal cross-sections of the join, Figure 4.4, shows the extent of the resin-rich regions in the seams on all three panels. Hand lay-up has, in some cases, caused two layers to overlap each other; the overall effect of this is a slight change in panel thickness in this area. Panels one and three both demonstrate this effect, both leading to

a slightly lower panel thickness at the seam (Fig.4.4: Table 4.2). In panel three the overlap appears to have blocked the resin flow to the gap left by ply eight and caused a void, this would cause a lowering of modulus if not masked by the 0° outer plies. The ply overlap in panel one has not had the same effect; this may be due to the size of the overlap being smaller. In the (0/30 – 0/20) seam in panel two a void has occurred without any ply overlap, in the sixth ply.

The reason for this is unknown but is likely due to the inherent difficulty for the resin to flow evenly throughout the laminate when the cross-linking reaction begins and viscosity rapidly increases.

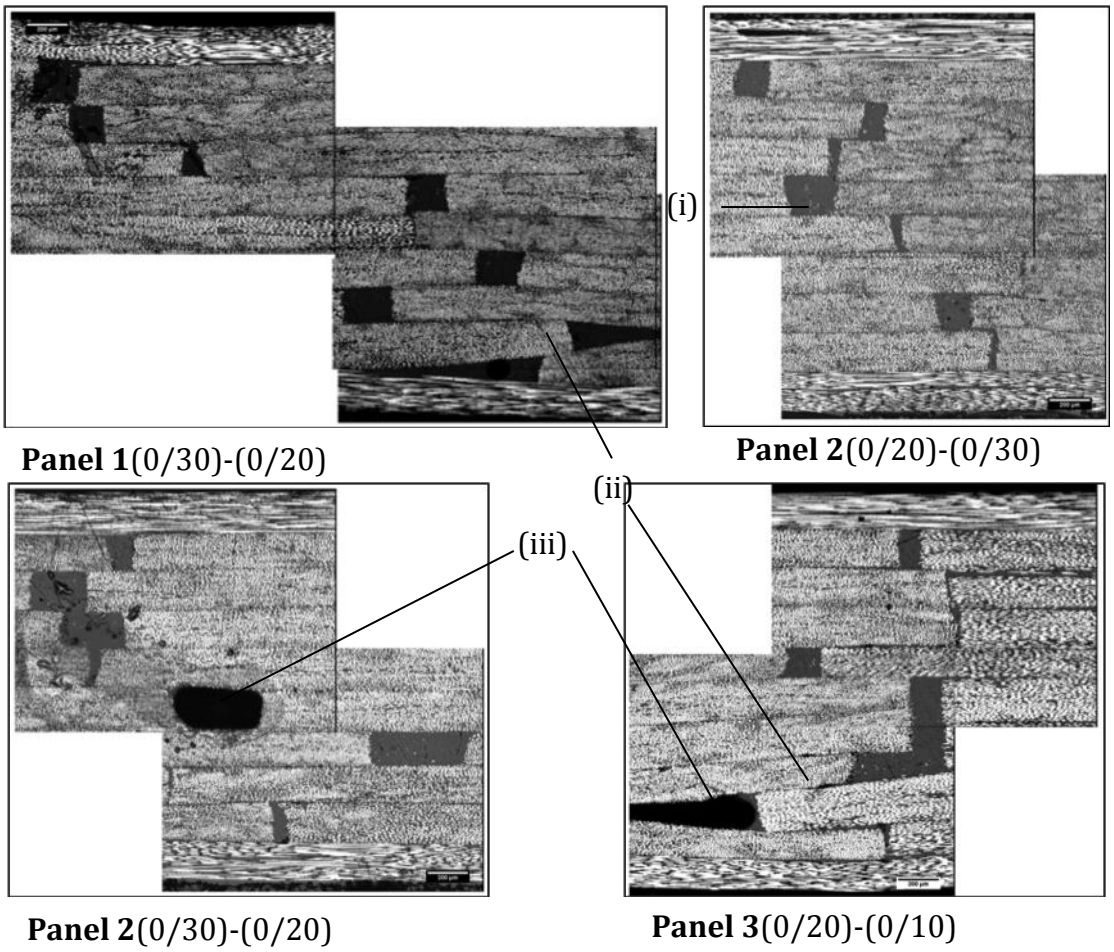

Figure 4.4 – Cross section of joins between sections in panels 1,2 and 3. Showing (i) resin rich regions, (ii) ply overlap and (iii) voids.

The void occurs in the largest cross-sectional area join between two plies (0.82 mm^2) across the three panels, a factor that cannot be overlooked. In the production of further sectioned laminates it is therefore key to make sure that no overlapping of sections occurs, yet they are as closely aligned as possible by careful alignment and accurate cutting.

Table 4.2 – Thickness at seam, ply overlap and resin rich regions of panels 1-3.

	Panel 1 (0/30)(0/20)	**Panel 2 (0/20)(0/30)(0/20)**		**Panel 3 (0/20)(0/10)**
	Seam 1	**Seam 1**	**Seam 2**	**Seam 1**
Thickness at seam (mm)	1.87	1.93	1.93	1.82
Resin rich region cross-sectional area (mm^2)	0.38	0.17	0.32	0.23
Ply overlap	8 & 9	-	-	7 & 8
Cross sectional area and location of voids (mm^2)	-	-	ply 6 - 81.7	ply 8 - 63.3

4 Control shafts

4.1 Methodology

Ten plies of 0° UD ACG MTM28/T800 composite were cut to 0.6 m lengths of increasing width in set increments, as the laminate would lay-up with increasing diameter from ply one to ten (Table 5.1). This ensured that the resulting composite consisted of the proposed ten plies, without regions of overlap that may lead to increased wall thickness or additional seams. The resulting shaft served as a control, with no sections of variation in lay-up. Three further sets of ten ply 0° UD ACG MTM28/T800 composite were then cut to consist of three distinct sections, 0.1 m, 0.1 m and 0.4 m in length respectively (C1, 2 and 3), (Figure 5.1). These provide nominally identical shafts, which serve as a baseline for the variable lay-up section shafts, showing any effect of the seam between sections. The three baseline shafts also served as a measure of manufacturing reproducibility when using multiple sections.

Table 5.1 – Dimensions of plies used to construct control shaft (C0).

Ply	New plies	Diameter (mm)	Width (mm)
1		22.5	70.686
2	1	22.75	71.471
3	2	23	72.257
4	3	23.25	73.042
5	4	23.5	73.827
6	5	23.75	74.613
7	6	24	75.398
8	7	24.25	76.184
9	8	24.5	76.969
10	9	24.75	77.754

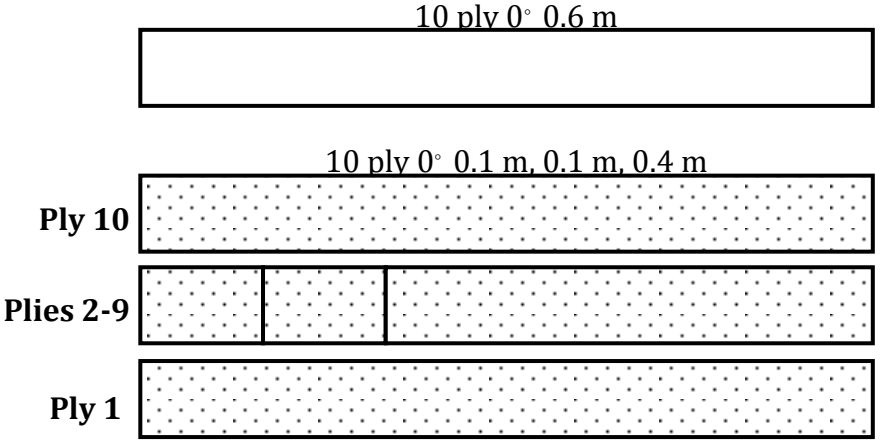

Figure 5.1 – Control (C1,2 & 3) 10 ply 0° 0.6 m and control with sections 10 ply 0° 0.1 m, 0.1 m, 0.4 m.

4.1.1 Manufacture

4.1.1.1 Hot pressing

The control shaft plies were then hand-laid up around a mandrel consisting of a aluminium alloy bar (Ø 0.016 m) core and a high temperature silicone tube (Ø 0.022 m, Width 0.003 m) (Figure 5.2). The silicone tube allow's the mandrel to be removed after pressing. Two plates of the aluminium alloy were used as the outer mould to be placed in the hot press (0.7 m x 0.7 m x 0.02 m). Channels of radius 0.0125 m were milled into each to produce a fully cylindrical mould of Ø 0.025 m when pressed together.

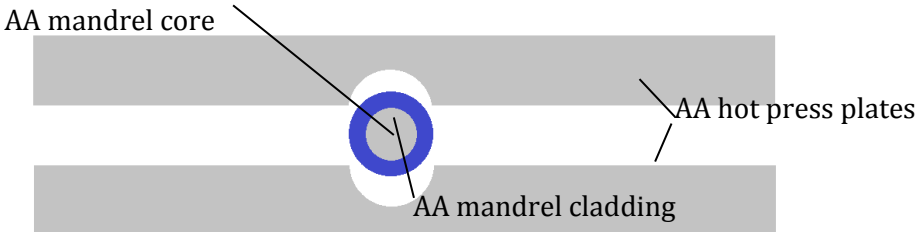

Figure 5.2 – Schematic diagram of hot press plates and mandrel arrangement.

The mandrel and hot press plates were coated in three layers of a liquid polymer release agent (Locktite Wollo) to prevent bonding to the epoxy resin and therefore ease the release of the cured shaft. The un-cured composite was placed between the hot press plates and clamped to 18 kN to ensure a consistent and controlled volume fraction, ply thickness and cross-section. The shafts were cured using a three stage thermal cycle; temperature was ramped up to 125 $^{\circ}$C at 0.5 $^{\circ}$C min^{-1}, held for 1 hour and then cooled at 3 $^{\circ}$C min^{-1} down to room temperature. Once cooled the clamping force was released and the shaft and mandrel removed from the mould. The silicone and aluminium alloy mandrel was then twisted and pulled out of the cured composite shaft, leaving an excellent internal and external surface finish.

4.1.2 Dimensions

Digital callipers (Mitutoyo Absolute Digimatic) were used to measure internal diameter, external diameter and wall thickness at both ends of each shaft (six per end), with continued external diameter measurements being made along and around the shaft (six at 0.1 m intervals).

4.1.3 Optical analysis

One end transverse section, obtained using a Buhler multi tool and a Struers Accutom was taken from the 0.6 m control shaft. Mounted in Durafix resin and polished to a 1 µm diamond paste finish. Samples were then inspected using a Zeiss microscope and Image J analysis software. The shaft was characterised for ply thickness, fibre volume fraction and overall wall thickness.

4.1.4 Quasi-static shaft flexure

Shafts were clamped in cantilever bending and loaded to 20 N over a span of 0.5 m, force and deflection were measured using an Instron 3345 and Bluehill software (Fig. 5.3). The loading and unloading cycle were both conducted at a rate of 10 mm/min, previous to which a pre-load of 0.5 N was applied. Ten cycles were conducted on each shaft and analysed for Young's modulus using $E = \frac{F\,l^3}{3\delta I}$ and $I = \frac{\pi}{4}({r_o}^4 - {r_i}^4)$.

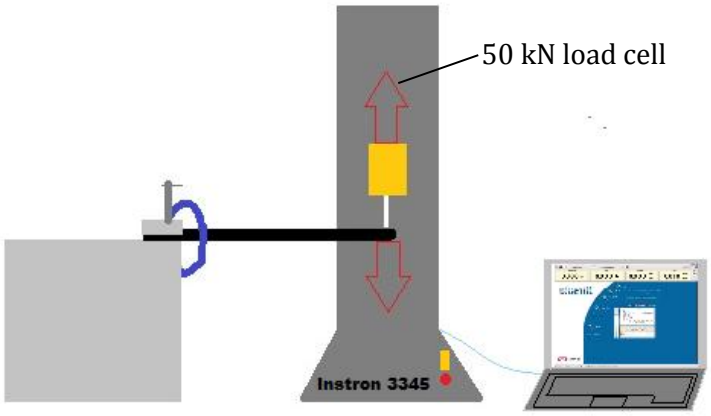

Figure 5.3 – Schematic diagram of the cantilever static shaft flexure using the Instron 3345 and Bluehill software.

4.2 Results and Discussion

4.2.1 Dimensions

The reproducibility of the manufacturing techniques used to produce the shafts needs to be high in order to control the factors affecting the modulus of different shafts. The measured dimensions of the shafts (Table 5.2) show limited scatter (diameter 25.34 ± 0.04 mm). The profile of the change in outer diameter along the shaft shows no significant effect with outer diameter remaining consistent (Fig. 5.4).

Table 5.2 – Dimensions and second moment of area of control shafts.

	Shaft			
	0	**0 sectioned 1**	**0 sectioned 2**	**0 sectioned 3**
Wall thickness (mm)	2.06 ± 0.05	2.155 ± 0.06	2.132 ± 0.04	2.134 ± 0.04
Inner diameter (m)	0.0117	0.0116	0.0116	0.0116
Outer diameter (m)	0.0128	0.0127	0.0127	0.0127
I (m^4)	6.10E-09	6.04E-09	6.06E-09	6.04E-09

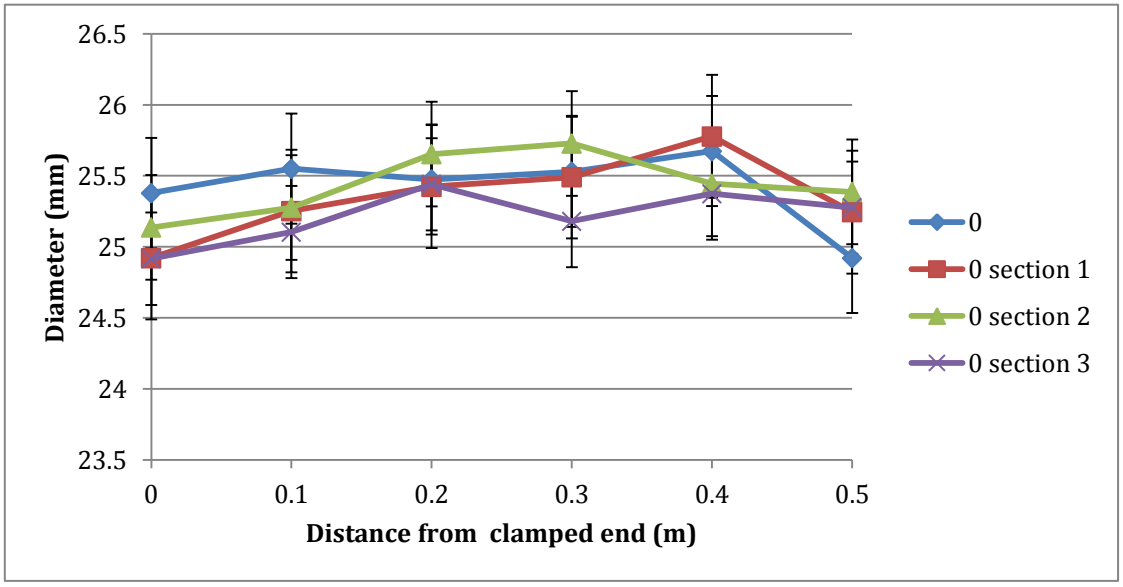

Figure 5.4 – Diameter of control shafts as a function of distance from clamped end.

4.2.2 Optical analysis

Image analysis was conducted on one sample only and only at the end of the shaft, as the shafts could not be sectioned as modulus testing was not complete. The sample showed consistent volume fraction and ply thickness throughout each of the plies (Table 5.3). The overall wall thickness was found to be within the standard deviation of that measured by the digital callipers (Mitutoyo Absolute Digimatic).

Table 5.3 – Average volume fraction, ply thickness and wall thickness for end of control shaft.

	Control Shaft
Volume fraction (%)	61.1 ± 4.6
Ply thickness (µm)	185 ± 26
Wall thickness (mm)	2.00 ± 0.03

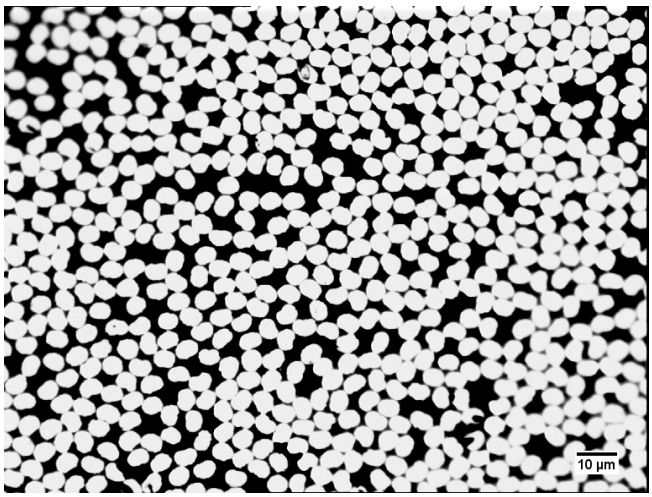

Figure 5.5 – Micrograph of fibre distribution a hot pressed composite.produces.

4.2.3 Quasi-static shaft flexure

The nominally identical shafts that had seams in two sections in plies 2 -8 showed consistent static bend behaviour. The three sectioned shafts in fact showed a higher average modulus than the control shaft (92.6 GPa and 81.1 GPa respectively). This is not a significant effect as figure 5.6 shows, the control shafts modulus was contained within the standard deviation of the sectioned shafts. It is important to note that the prediction of the modulus of the shafts from previous panel testing input into CoDA (97.3 GPa) was also within the standard deviation of the sectioned shafts tested. The most important outcome of the static bend testing was therefore that the seam evident between the sections has no effect on the static modulus of the shafts, although scatter does increase with use of multiple sections.

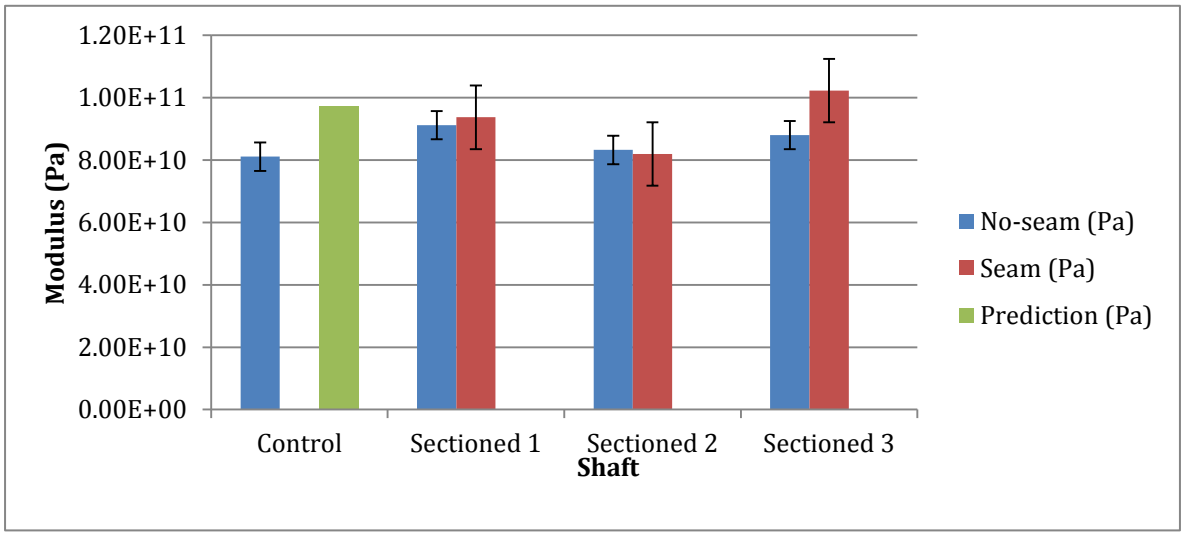

Figure 5.6 – Modulus of control and sectioned shafts in sections with and without seam compared to the CoDA prediction of modulus.

5 Multiple section shafts

5.1 Methodology

5.1.1 Manufacture

Five shafts with multiple sections of ten ply UD ACG MTM28/T800 composite were cut to relevant orientations and lengths (Figure 6.1). Each ply increased in width in set increments, as the laminate would lay-up with increasing diameter from ply one to ten (Table 6.1). This ensured that the resulting composite consisted of the proposed ten plies, without regions of overlap that may lead to increased wall thickness or additional seams. Figure 6.2 shows an example of how the multiple section shafts were laid-up with continuous 0° fibres in plies 1 and 10 and off axis plies of each section between them.

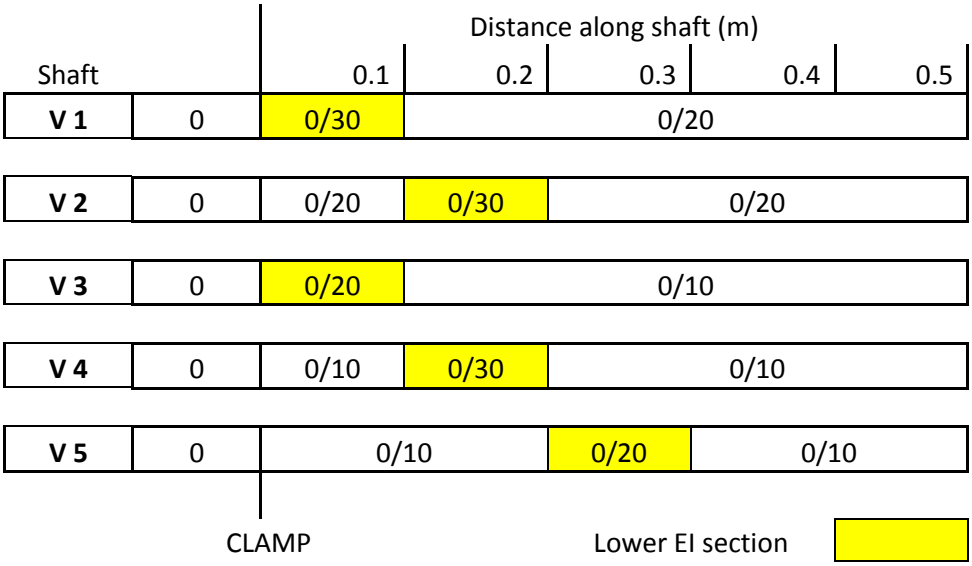

Figure 6.1 – Multiple section shaft's V 1-5, showing lower EI section placement and overall lay up of shaft.

Table 6.1 – Dimensions of plies used to construct multiple section shaft's (V 1-5).

Ply	New plies	Diameter (mm)	Width (mm)
1		22.5	70.69
2	1	22.75	71.47
3	2	23	72.26
4	3	23.25	73.04
5	4	23.5	73.83
6	5	23.75	74.61
7	6	24	75.40
8	7	24.25	76.18
9	8	24.5	76.97
10	9	24.75	77.75

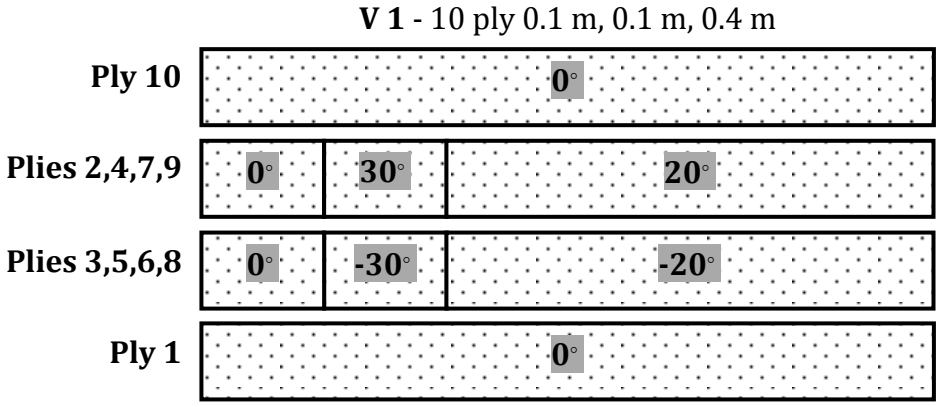

Figure 6.2 – Schematic diagram of example multiple section shaft (V 1) lay- up, 10 ply 0° 0.1 m, 0.1 m, 0.4 m.

5.1.2 Hot pressing

The multiple section shaft plies were then hand-laid up around a mandrel consisting of an aluminium alloy bar (Ø 0.016 m) core and a high temperature silicone tube (Ø 0.022 m, wall thickness 0.003 m) (Fig. 6.3). The silicone tube allows the mandrel to be removed after pressing. Two plates of aluminium alloy were used as the outer mould to be placed in the hot press (0.7 m x 0.7 m x 0.02 m). Channels of radius 0.0125 m were milled into each to produce a fully cylindrical mould of Ø 0.025 m when pressed together.

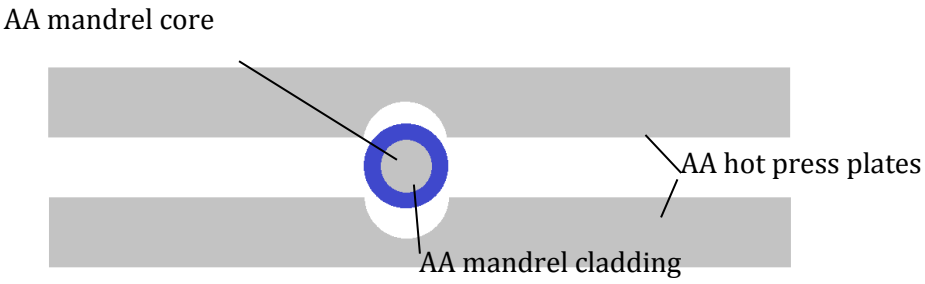

Figure 6.3 – Schematic diagram of hot press plates and mandrel arrangement.

The mandrel and hot press plates were coated in three layers of a liquid polymer release agent (Locktite Wolo) to prevent bonding to the epoxy resin and therefore to

ease the release of the cured shaft. The un-cured composite was placed between the hot press plates and clamped to 20 kN to ensure a consistent and controlled volume fraction, ply thickness and cross-section. The shafts were cured using a three stage thermal cycle; temperature was ramped up to 125 °C at 0.5 °C min^{-1}, held for 1 hour and then cooled at 3 °C min^{-1} down to room temperature. The temperature cycle for shaft V2 was monitored using a thermocouple (RS-1315) attached to the heated platens to verify the curing cycle (Fig. 6.4). The cycle showed good replication of the thermal cycle used for vacuum bagged composite production.

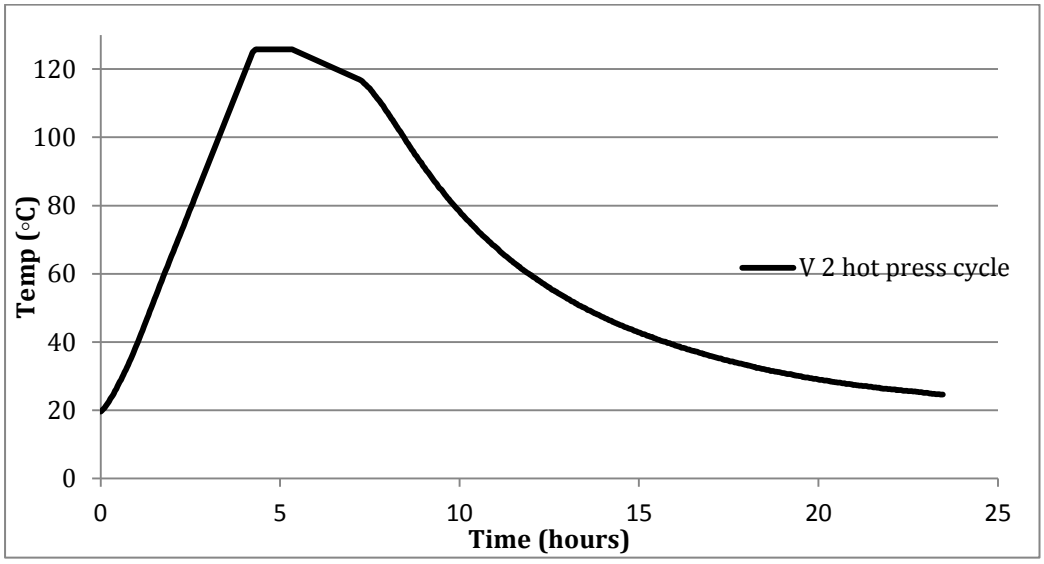

Figure 6.4 – Temperature vs. time for curing cycle of shaft V 2 in hot press.

Once cooled the clamping force was released and the shaft and mandrel removed from the mould. The silicone and aluminium alloy mandrel were then twisted and pulled out of the cured composite shaft, leaving an excellent internal and external surface finish.

5.1.3 Dimensions

Digital callipers (Mitutoyo Absolute Digimatic) were used to measure internal diameter, external diameter and wall thickness at both ends of each shaft (six per end), with continued external diameter measurements being made along and around the shaft (six at 0.1 m intervals). Once the shafts had been full characterised statically and dynamically they were sectioned at 0.1 m increments in order to create a wall thickness profile and a more accurate second moment of area value.

5.1.4 Quasi-static shaft flexure

Shafts were clamped in cantilever bending and loaded to 20 N over a span of 0.5 m, and then decreasing increments of 0.1 m from the clamp. Force-deflection data at 0.2, 0.3, 0.4 and 0.5 m from the clamp were measured using an Instron 3345 and Bluehill software (Fig. 6.5). The loading and unloading cycle were both conducted at a rate of 10 mm/min, previous to which a pre-load of 2 N was applied. Ten cycles were conducted at each point on each shaft and analysed for Young's modulus using $E = \frac{F\,l^3}{3\delta I}$ and $I = \frac{\pi}{4}({r_o}^4 - {r_i}^4)$ and deflection profile by the maximum deflection under a load of 20 N at each point. Initially, the effect of the presence and position of the lower EI section on the static deflection profile was investigated.

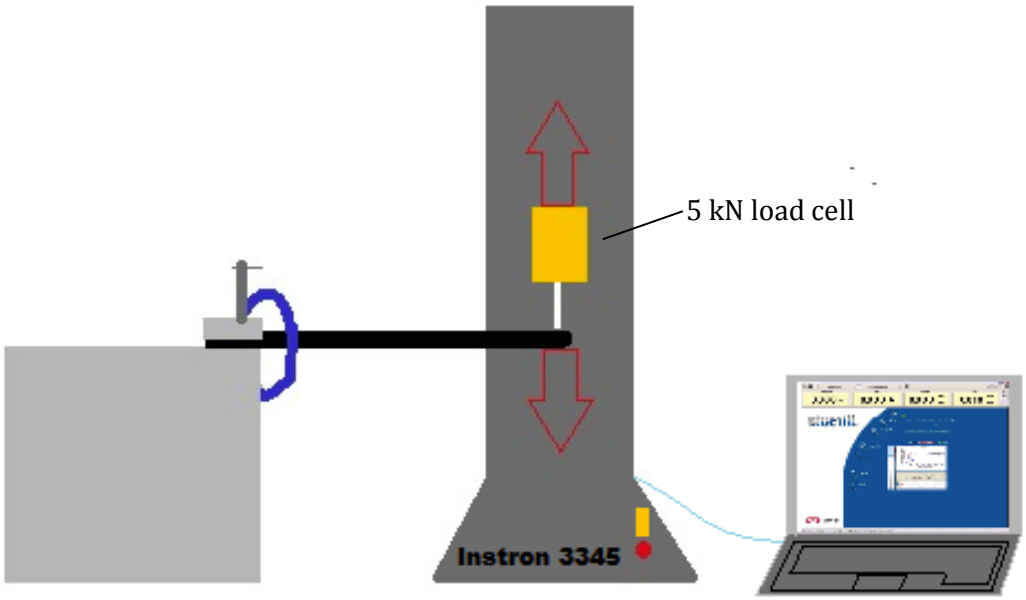

Figure 6.5 – Schematic diagram of the cantilever static shaft flexure using the Instron 3345 and Bluehill software.

5.1.5 Dynamic drop-ball shaft flexure

To analyse the dynamic behaviour of the multiple sectioned shafts, they were clamped in a cantilever bend (0.5 m) identical to the quasi-static testing. Clear white markings were placed at 0.1, 0.2, 0.3, 0.4 and 0.5 m away from the clamped end so to produce distinct points for the Phantom V7.3 high speed camera and Phantom camera control software to identify. A Mercian Spider Dimple hockey ball (0.16 kg) was used to impact the shafts vertically from a range of heights, and therefore impact force (Fig. 6.6). The resulting shaft deflection was recorded at 6600 fps and then analysed using a combination of Tracker and Phantom software. Each shaft was evaluated for maximum deflection at 0.1 m increments along the shaft, impact force and therefore stiffness, flexural rigidity and modulus and finally CoR. Impact force was determined by the negative acceleration of the ball from initial contact with the shaft to maximum deflection using: $a = (v - u) / t$ and $F = ma$ where;

a = acceleration (ms^{-2})
v = final velocity at maximum deflection
i.e. Rest (ms^{-1})
u = impact velocity (ms^{-1})
t = time from impact to maximum deflection (s)
F = force (N)
M = mass of hockey ball (kg)

CoR was determined by the conversion of inbound ball speed (V_{in}) to outbound ball speed (V_{out}) by the equation $CoR = \frac{V_{out}}{V_{in}}$. The CoR was expected to be a function of overall shaft stiffness, increasing as stiffness does. The dynamic deflection profile of the shaft at maximum negative deflection and positive deflection should give an indication into the bending behaviour of the shafts and whether it is possible to identify a bend or "kick point" and whether the position of the lower EI section has an effect on this.

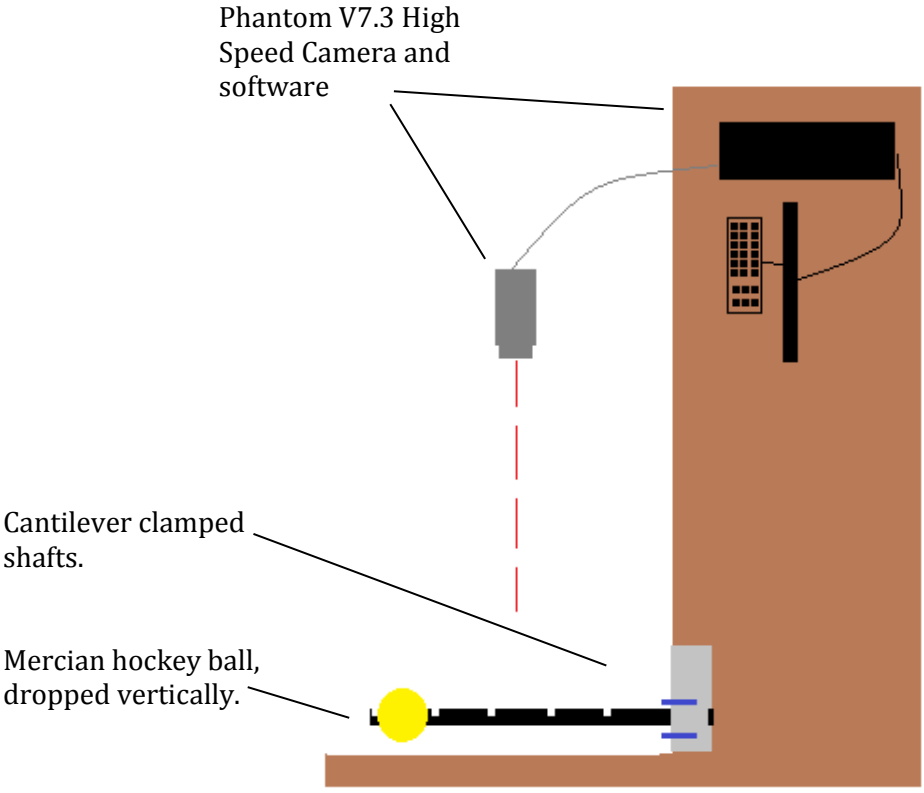

Figure 6.6 – Schematic representation of the dynamic drop-ball shaft flexure testing, using Phantom V 7.3 High speed camera and software.

5.1.6 Strain distribution

5.1.6.1 Quasi-static flexure

Shafts C 0, C 3 And V 1-5 were clamped in cantilever bending over a span of 0.5 m and loaded to 30 N, the load was held here for 30 seconds to allow stain data to be acquired from stain gauges (Kyowa – KFG-2-120-C1-11L1M2R) positioned at key points along the shafts (Table. 6.2). These key points on the multiple section shafts coincided with the seams between sections and in both the lower EI and main sections of the shafts. Strain data were analysed at 100 Hz through a PCD-300A interface box and PCD-30A analysis software.

Table 6.2– Position of strain gauges for quasi-static and dynamic analysis.

	Strain gauge position from clamp (m) - X denotes seam position						
Shaft	0.05	0.1	0.15	0.2	0.25	0.3	0.35
C 0	X	X	X	X	X	X	X
C 3	X	X				X	
V 1	X	X				X	
V 2	X	X	X	X			X
V 3	X	X				X	
V 4	X	X	X	X			X
V 5	X	X		X	X	X	X

5.1.6.2 Dynamic drop-ball flexure and Frequency analysis

Shafts C 0, C 3 and V 1-5 were clamped at 0.5 m span cantilevers (as in quasi-static testing) with stain gauges also in the same position (Table. 6.2). A Mercian Spider Dimple hockey ball (0.16 kg) was used to impact the shafts vertically from no higher than 0.5 m and the stain data recorded at 5000 Hz through a PCD-300A interface box and PCD-30A analysis software.

Acquired stain data from the quasi-static and dynamic testing were analysed for the distribution of strain throughout the shaft and the impact of the seams and lower EI sections.

The shafts were also evaluated for their fundamental bending frequency and therefore modulus (E) through the relationship $E = \frac{m_0 \, l^4 \, x \, (\frac{f_1 \, 2\pi}{C_1})^2}{I}$.

Where:

f_1 = Mode 1 bending frequency (s^{-1})

C_1 = 3.52

m_0 = ρ / A (kg m^{-1})

ρ = Density (kgm^{-3})

A = Section area (m^2)

I = Second moment of area (m^4)

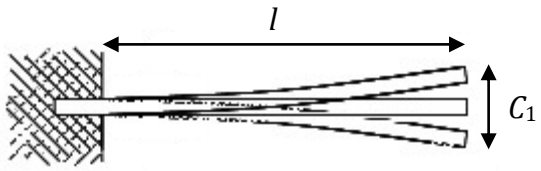

5.1.7 Optical analysis

Twenty three samples from the multiple sectioned and control shafts in longitudinal and transverse cross-sections were obtained using a Buhler multi tool and a Struers Accutom. Transverse cross sections were taken from the different lay-up sections and the longitudinal cross-sections were taken from the seam at which they join. They were mounted in Durafix resin and polished to a 1 µm diamond paste finish. Samples were then inspected using Zeiss microscope and Image J analysis software. The shafts were characterised for ply thickness, fibre volume fraction, ply orientation and seam cross-section.

5.2 Results and Discussion

5.2.1 Dimensions

The reproducibility of the manufacturing techniques used to produce the shafts needs to be high in order to control the factors affecting the modulus of different shafts. The measured dimensions of the shafts (Table 6.3) show limited scatter (diameter 25.30 ± 0.02 mm). The profile of the change in outer diameter along the shaft shows a slight increase in diameter towards the centre in all but shaft V 1. V 1 was cured under a lower load than shafts V 2, V 4 and V 5, this was due to a fault in the hot press. The effect of this only appears to be at lengths between 0 and 0.3 m where average diameter is up to 0.4 mm larger than shafts V 2 – V 5. An explanation for this could be that due to the hot press fault, there was uneven loading on this shaft, not consolidating the plies in this region and could lead to a lower volume fraction; this will be investigated through optical microscopy. Taking this into account the scatter between shafts V2 –V5 is low and diameter profile follows a similar trend (Fig. 6.7). There was also a fault on the hot press during the production of shaft V 3 which led to its higher wall thickness and second moment of area values. The distribution of the increased diameter, however, is different to that of shaft V 1 in that it shows the totally opposite diameter profile.

The wall thickness values obtained from both ends of the shafts are significantly higher than those used to model the behaviour of the shafts. The average wall thickness produced from shafts in the hot press is 2.13 ± 0.08 mm whereas the wall thickness used in the modelling stage, derived from given single ply thickness values of the MTM28/High Strength-T800 carbon fibre composite was 1.25 mm. The average ply thickness obtained from initial optical microscopy conducted on shaft C 0 showed an average ply thickness of 185 ± 26 μm, a significant increase from 125 μm.

Table 6.3– Dimensions and second moment of area of shafts.

	Shaft								
	C 0	**C 1**	**C 2**	**C 3**	**V 1**	**V 2**	**V 3**	**V 4**	**V 5**
Wall thickness (mm)	2.12	2.16	2.13	2.13	2.22	2.01	2.28	1.97	2.11
Standard deviation (mm)	0.00005	0.00007	0.00004	0.00004	0.00018	0.00004	0.00014	0.00009	0.00010
Inner diameter (mm)	23.40	23.20	23.20	23.20	21.00	21.00	20.80	23.20	23.20
Standard deviation (mm)	0.05	0.07	0.04	0.04	0.18	0.04	0.14	0.09	0.10
Outer diameter (mm)	25.52	25.32	25.42	25.32	21.07	21.07	25.40	25.20	25.20
Standard deviation (mm)	0.39	0.43	0.37	0.32	0.28	0.22	0.24	0.32	0.29
I (m^4)	5.97E-09	6.04E-09	6.06E-09	5.99E-09	6.34E-09	5.82E-09	6.33E-09	5.47E-09	5.88E-09

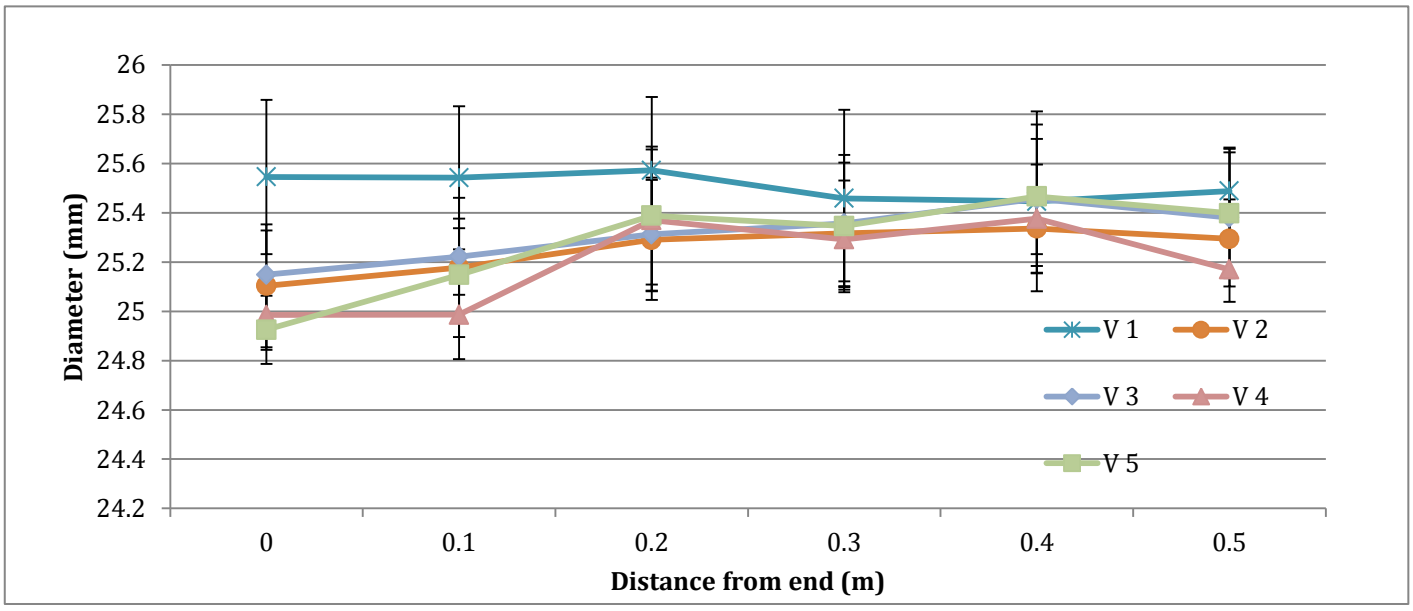

Figure 6.7 – Diameter of control shafts as a function of distance from clamped end.

5.2.2 Quasi-static shaft flexure

A summary of the quasi-static bend tests conducted on shafts V 1 – V 5 are shown in Table. 6.4. It shows the predicted values, experimentally derived values and the % difference between these for both the overall flexural rigidity (EI/Nm^2) and modulus (GPa). The results show that the CoDA and adapted Broulliette's equation modelling of overall shaft flexural rigidity under-predicted the EI values, but over-predicted the modulus values. The greater second moment of area in shaft's V 1-5 than was used in the original model contributed to the higher EI values seen in all the shafts. For a shaft of diameter 25 mm and wall thickness of 1.25 mm (10 plies at given ply thickness of MTM28/High Strength-T800) the second moment of area is 6.59 x10^{-9} m^4. The average second moment of area for the shafts produced in the hot press is however 1.05 x10^{-8} m^4, a significant increase. This value has been obtained from wall thickness values at both ends of the shafts only and will need to be reviewed on sectioning of the shafts to identify a wall thickness profile and a more accurate overall second moment of area.

Table 6.4 – Summary of static shaft flexure of shafts V 1 – V 5.

	Shaft				
	V 1	**V 2**	**V 3**	**V 4**	**V 5**
Experimental EI (Nm^2)	582.42	593.15	481.88	666.45	728.52
Stdev	0.61	1.74	0.91	1.37	1.58
Predicted EI (Nm^2)	418.77	493.09	535.72	575.79	603.75
% difference	39.08	20.29	-10.05	15.75	20.67
Experimental moduli (GPa)	52.44	57.76	43.68	68.64	70.32
Stdev	0.05	0.17	0.08	0.14	0.15
Predicted moduli (GPa)	63.54	74.82	81.30	87.37	91.61
% difference	-17.47	-22.80	-46.27	-21.44	-23.24

The fault in the hot pressing in shaft V 3 contributing to an above average second moment of area and wall thickness, usually associated with creating a stiffer section. The experimental values of flexural rigidity or modulus values were well below those of the other shafts and the predicted values. The reason for this will

be investigated when optical microscopy is conducted on the shafts. The surface finish of shaft V 3 is noticeably different to shafts V 1, 2, 4 and 5 and appears to have higher resin content contributing to a duller exterior. As the clamping conditions were not good enough for the resin to be forced against the mould, along the fibres and out at each end. The relationship between predicted and experimental modulus (a) and flexural rigidity (b) in shafts V 1-3 is represented in Fig. 6.8.

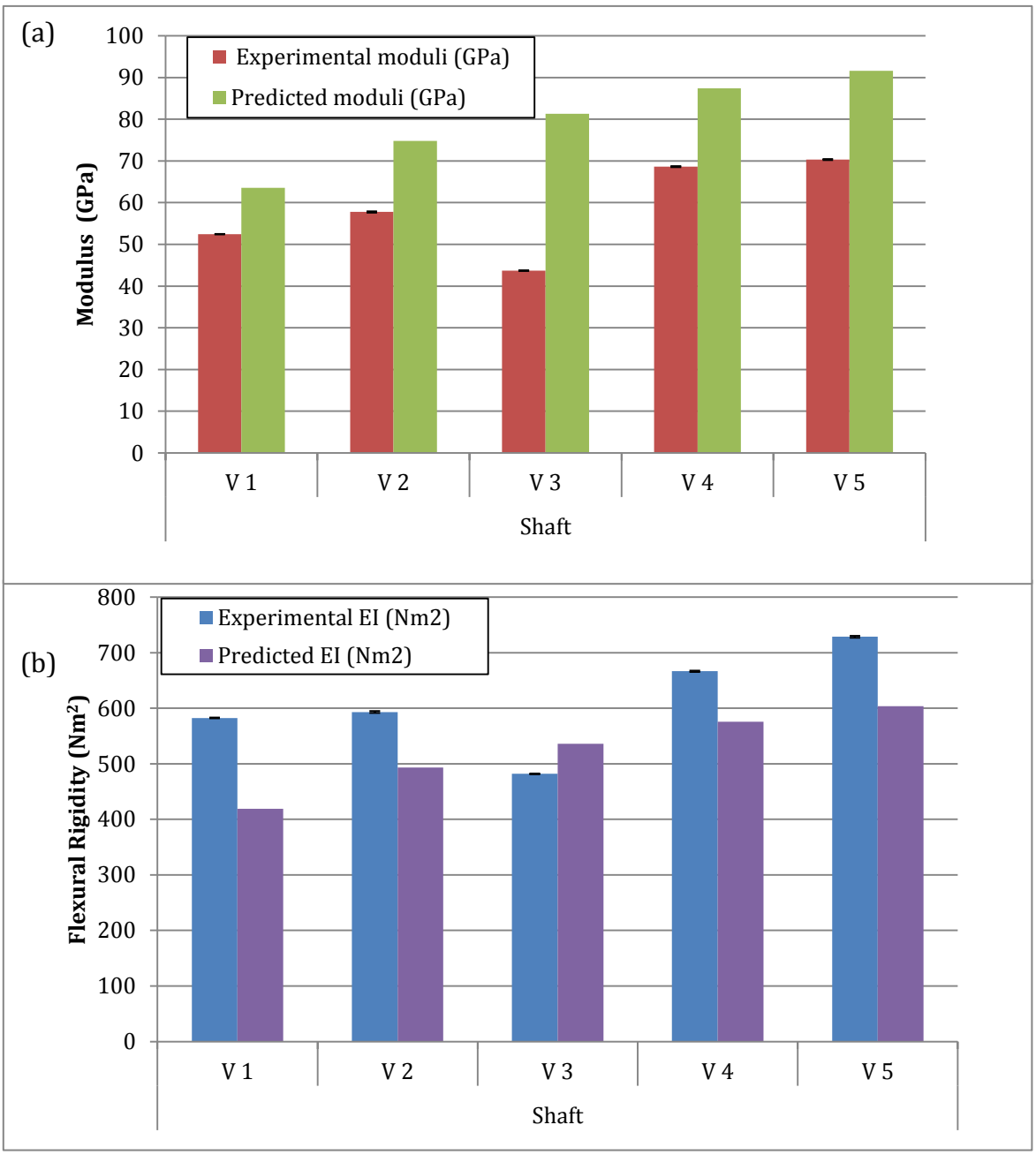

Figure 6.8 – Relationship between predicted and experimental (a) modulus and (b) flexural rigidity values for shafts V 1-3.

Along with overall shaft flexure, repeat tests were also conducted at decreasing cantilever lengths of 0.4, 0.3 and 0.2 m. An example of the stiffness behaviour at each point in shaft V 2 is shown in Fig. 6.9.

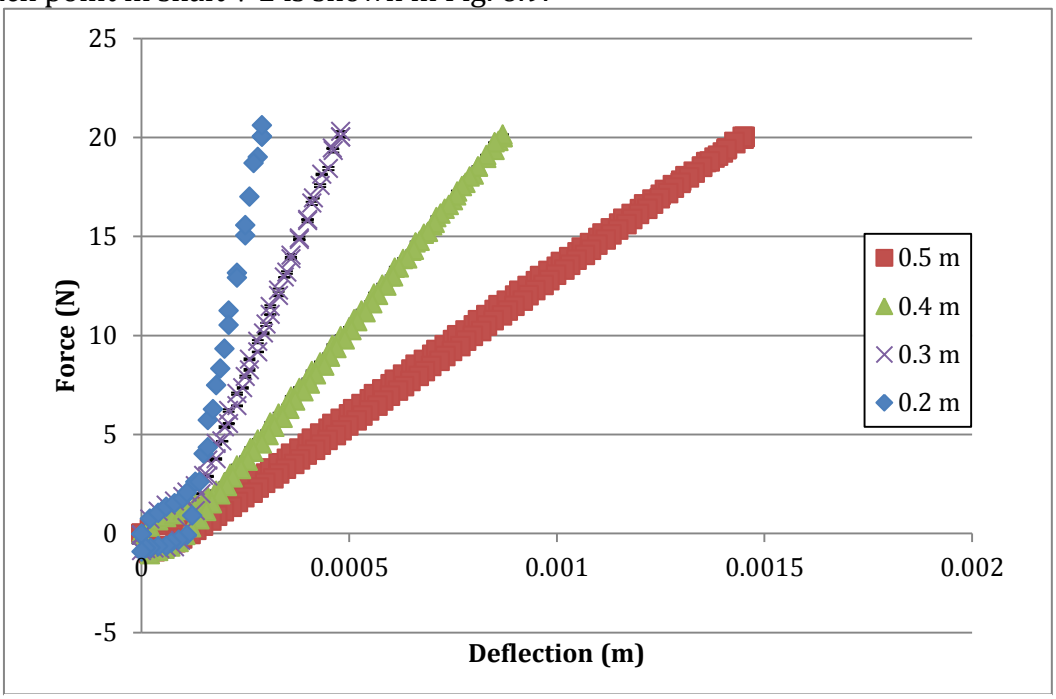

Figure 6.9 – Force-deflection curve's for shaft V 2 at 0.2, 0.3, 0.4 and 0.5 m cantilever lengths.

As expected, with decreasing cantilever length, the stiffness increases. However, it is necessary to analyse the relative changes between shafts in order to determine the effects of the different multiple sections on local stiffness. The percentage increase in stiffness, with respect to the stiffness of the 0.2 m section, from each cantilever length to the next is shown in Table 6.5 and Fig. 6.10. In shafts V 1 – 4 there is no significant difference in the proportional change in the stiffness of different sections. Suggesting that the presence of the lower EI section has no effect on the overall quasi-static bend behaviour in these shafts. There is however, a proportional change in stiffness of shaft V 5. The stiffness at a cantilever length of 0.3 m, the point at which there is a seam is significantly lower, as a percentage of the maximum stiffness (43.7 %). This is the only shaft in which the cantilever bend at 0.2 m is over just one single section, of 0/10° lay-up. Then when loaded at 0.3 m, the lower EI 0/20° section and the seam between them is taken into account and therefore creating a larger decrease in stiffness than was evident in the shafts that are already being loaded over multiple sections at a cantilever length of 0.2 m. The stiffness values at cantilever lengths

0.4 m and 0.5 m are also significantly higher (27.2 and 16.2 %) when compared to shafts V 1 - 4 (Table 6.5, Fig. 6.10). This could be due to the point at which bending, or maximum strain is occurring, if the maximum strain point is moved down the shaft by the lower EI section (between 0.2 and 0.3 m), then this could have an impact on the effective cantilever length of the shaft. It is expected, in uniform parallel sided shafts, loaded in cantilever for maximum strain to occur next to the clamp and therefore controlling the stiffness as the full length of the shaft is being strained a uniformly decreasing amount. If maximum strain does not occur next to the clamp then the effective cantilever length is decreased and therefore increasing the measured stiffness.

Table 6.5 – Percentage decrease in stiffness as cantilever length increases in shafts V 1-5.

	Position (m)			
	0.2	**0.3**	**0.4**	**0.5**
V 1 (N/m)	105586.71	48307.53	24681.25	14406.01
%	100.0	54.2	23.4	13.6
V2 (N/m)	112837.92	52204.69	25871.88	14671.26
%	100.0	53.7	22.9	13.0
V3 (N/m)	89130.87	41882.69	20525.47	11919.11
%	100.0	53.0	23.0	13.4
V4 (N/m)	125467.36	58195.80	27945.86	16484.37
%	100.0	53.6	22.3	13.1
V5 (N/m)	111226.90	62671.38	30229.25	18019.67
%	100.0	43.7	27.2	16.2

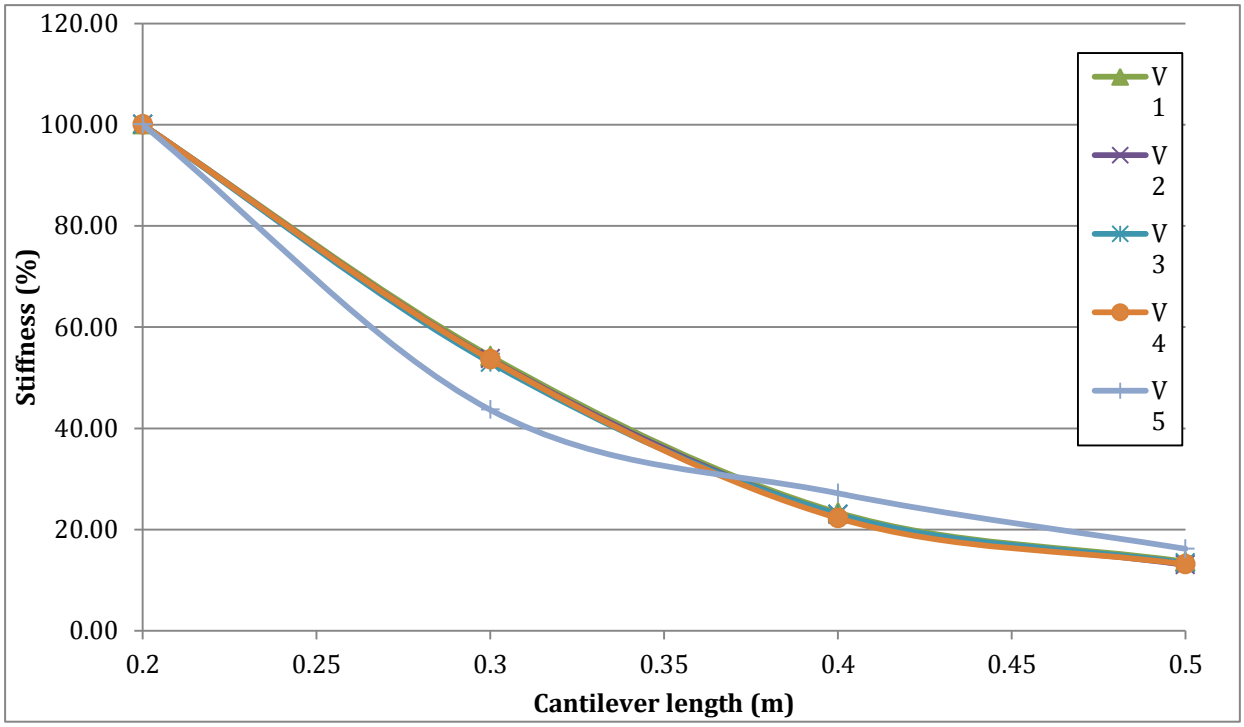

Figure 6.10 – Profile of percentage decrease in stiffness as cantilever length increase's in shafts V 1-5.

The deflection profile of these shafts under 20 N load at each cantilever length was compared to the profile determined for the control shafts C 0 and C 3 (Fig. 6.11).

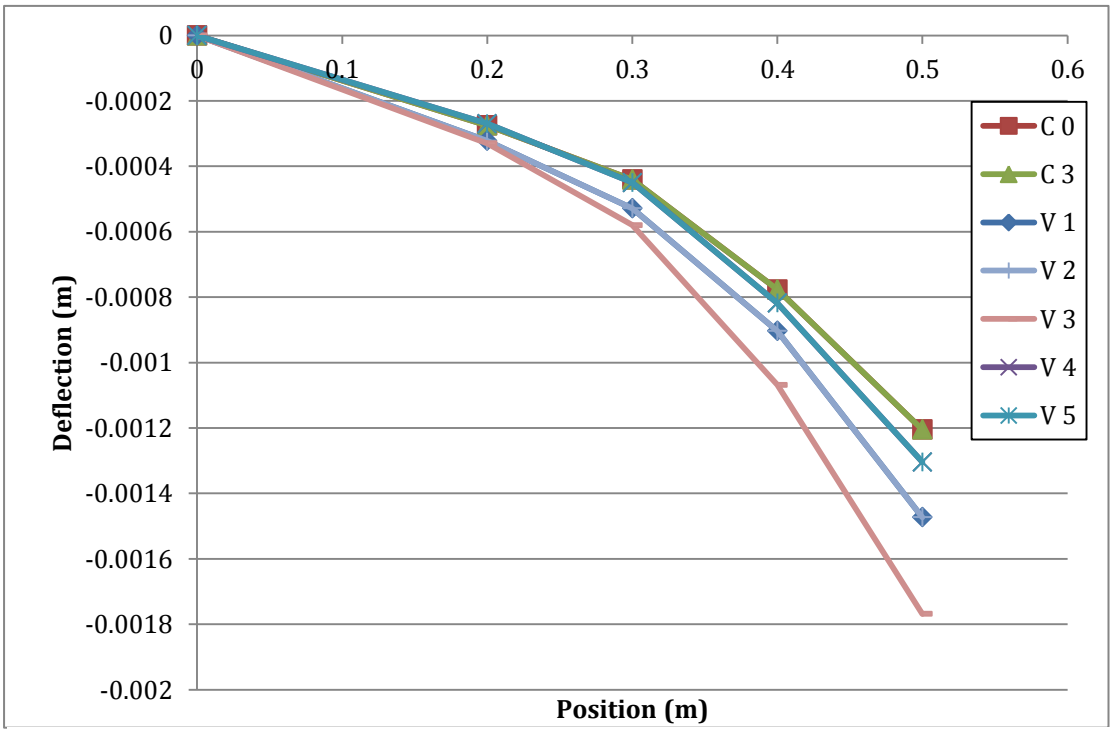

Figure 6.11 – Deflection profile under 20 N maximum load in shafts V 1-5 and C 0-3.

The deflection profile of the control shafts C 0 and C 3 shows little scatter, indeed shafts V 1 and 2 also show an identical profile of maximum deflection under 20 N load. It is interesting to see that at 0.2 m cantilever bend shafts V 1-3 are very closely matched; however the lower flexural rigidity and modulus shaft V 3 then starts to deflect more with respect to V 1 and 2. This suggests that it is at this point that the shaft strains the most and where bending is controlled from. A similar effect can be seen in shafts C 0, 3 and V 5. They all show a closely matched deflection profile up to 0.3 m cantilever length, then at this point shaft V 5 begins to deviate away from the control shafts and deflect a greater amount. Developing on from the discussed impact of the lower EI section and the seams in this shaft. Quasi-static testing with strain gauge data will be conducted to understand this further.

5.2.3 Dynamic drop-ball shaft flexure

In dynamic testing shafts C 0 -3 and V 1-5 showed a much lower modulus when compared to quasi-static testing. This could be due to the use of maximum deflection, but only average applied force. They did however follow similar trends in terms of the relationship between the shafts. Shaft C 0 showed the highest modulus from the dynamic testing (65.35 ± 4.13 GPa), followed closely by C 3 (63.41 ±3.09 GPa). The conversion of this modulus into dynamic ball interaction gave these shafts a CoR of 0.50 and 0.39 respectively, a concurrent drop in CoR with the presence of the seam in C 3. The ability of the multi-sectioned shafts V 1-5 of converting inbound ball speed into outbound ball speed differed from that of the control shafts. Even though shafts V 1-5 displayed a lower modulus, they did in fact have a higher CoR than the control shafts in some cases. There is a good relationship between the modulus of all the multi-

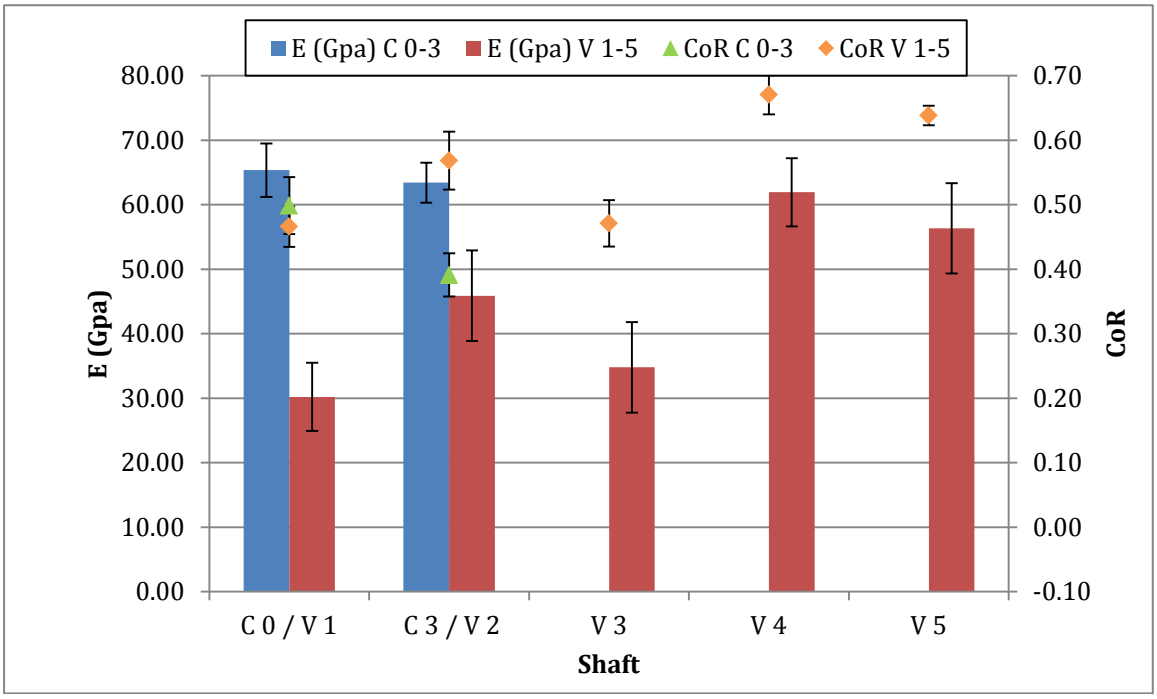

Figure 6.12 – Dynamic modulus and CoR values for control and multi-sectioned shafts.

sectioned shafts, as modulus increases so does CoR and vice-versa (Fig. 6.12).

To understand what is happening to the shafts during deflection and subsequent release of the ball at impact, Tracker software was used to track points at 0.1, 0.2, 0.3, 0.4 and 0.5 m from the clamp. The bending profile of the shaft would give an indication of the bend point and the extent to which the position of seams and lower EI sections affects this. The data acquired from Tracker are displayed

in Fig. 6.13, but it is certainly not conclusive. There does not appear to be a difference in the deflection profile between the control (a) and multi-sectioned (b) shafts. Deflection in the negative direction following ball impact and the subsequent positive deflection at ball release show a high scatter and do not display any noticeable relationships. For this reason dynamic data will be acquired using strain gauges at key points along the shafts to fully determine the dynamic behaviour.

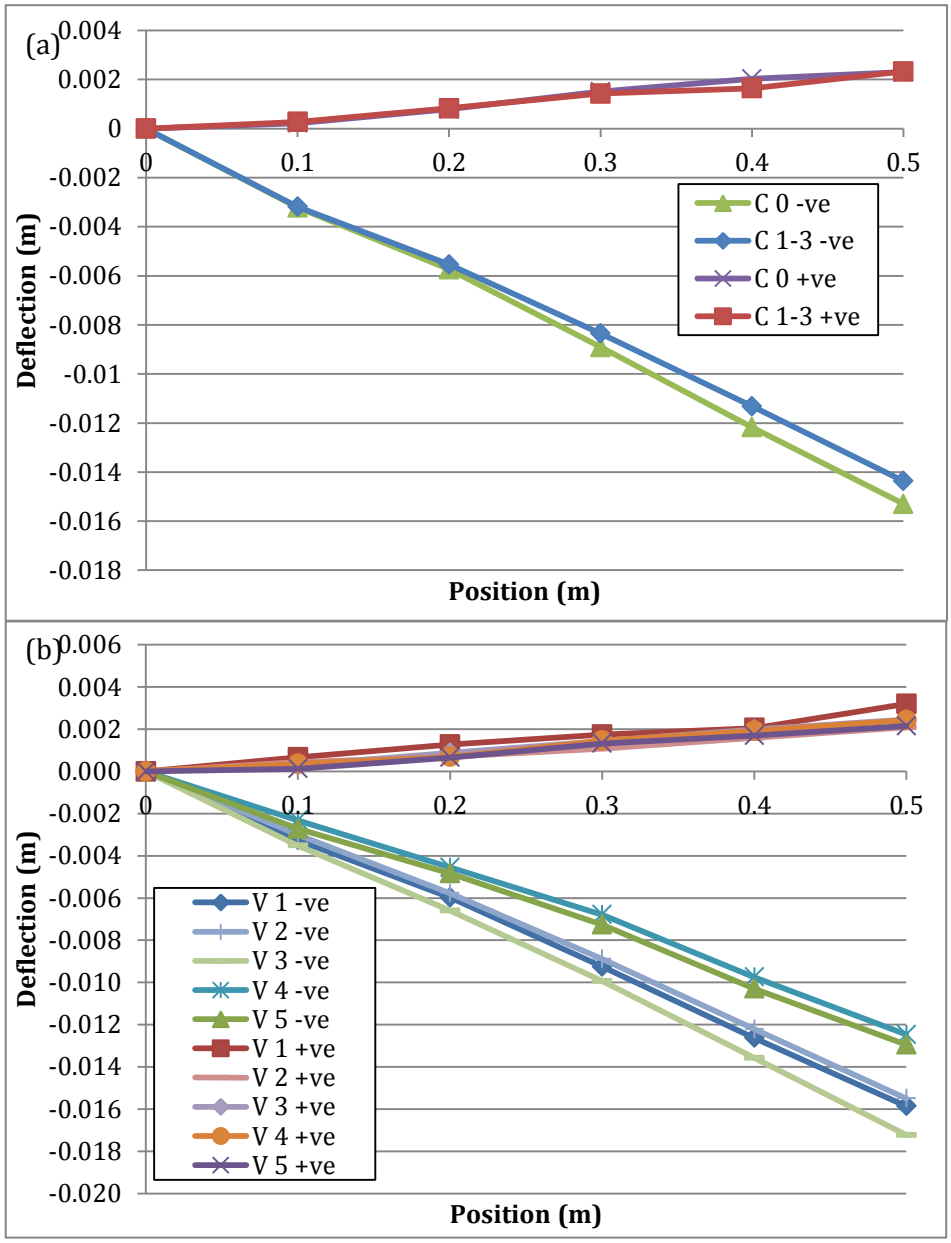

Figure 6.13 – Maximum negative and positive dynamic deflection profile for control (a) and multi-sectioned (b) shafts.

5.2.4 Strain distribution

5.2.4.1 Quasi-static flexure

The distribution of strain in C 0 was as expected, with maximum strain occurring at 0.05 m away from the clamp and then decreasing as distance away from the clamp increases, creating a parabolic deflection profile (Fig. 6.14). In the control multiple section shaft C 3 the strain in the seam at 0.1 m down the shaft was higher than at 0.05 m and also at 0.3 m. Suggesting that the bending behaviour of the shafts is affected by the presence of a seam alone, however this effect was not present in the multiple sectioned shafts V 1 and 3 which have a seam in the same position.

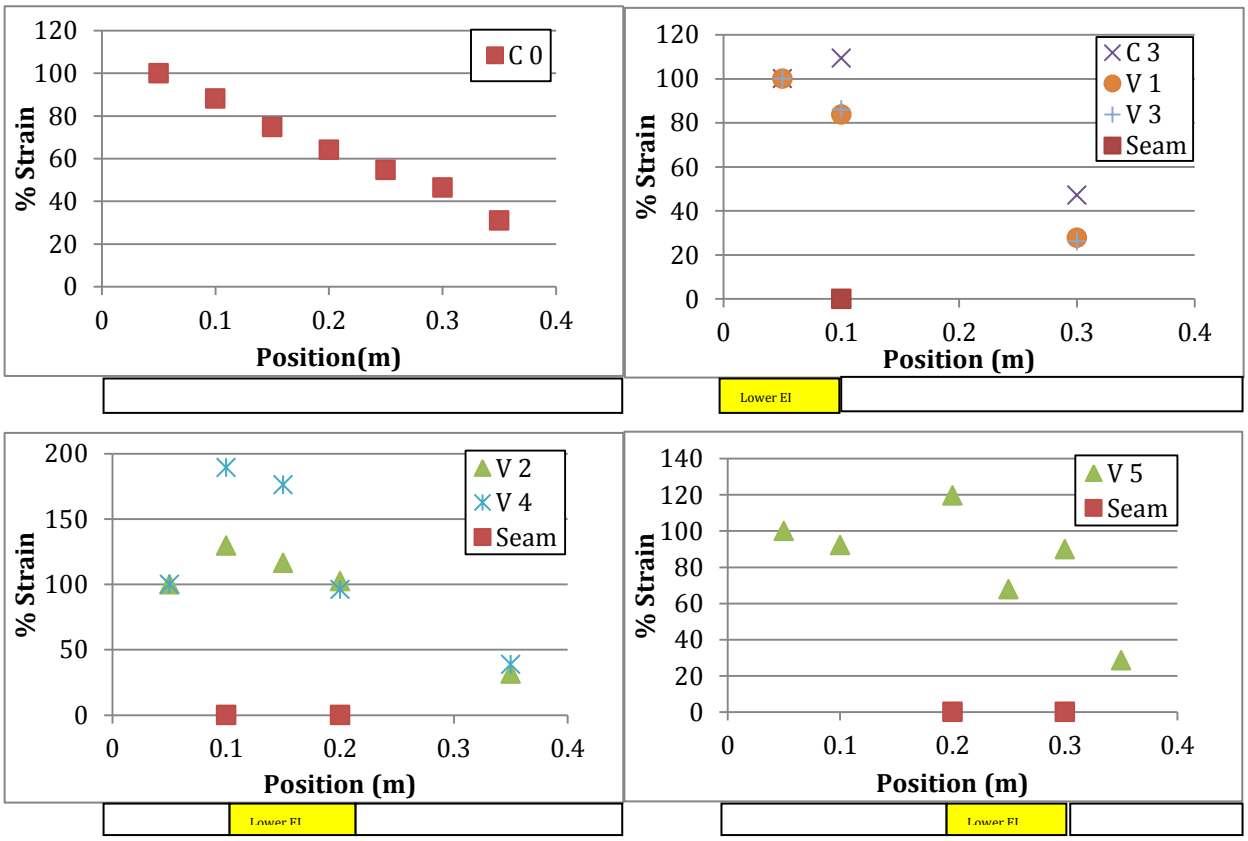

Figure 6.14 – Percentage strain as a function of distance from the clamp in shafts C 0, C 3 and V 1-5 under static deflection at 30 N load. With reference to seam's and lower EI sections.

In shafts V 2 and V 4 the maximum strain occurs at the seam at 0.1 m away from the clamp, with strain almost double that at 0.05 m in V 4. The lay-up of the multiple sections in these shafts is similar in position and the lower EI section is the same (0/30˚). The main body of the shaft however, has a different lay-up and this helps to explain why there is such a larger increase in strain in the 0/30˚ in the V 4 shaft. The 0/10˚ lay-up in the main body of V 4 is inherently stiffer than the 0/20˚ lay-up in the main body of V2. So the relative increase in strain between 0.05 m and 0.1 m in shaft V 4 is due to the Lower EI section having a much lower stiffness than the main body of the shaft. The strain distribution in shaft V 5 develops on the behaviour of the previous shafts. The maximum strain occurs at the seam at 0.2 m away from the clamp, with another peak in strain at the seam 0.3 m away from the clamp. So the position of the lower EI section, by introducing the seams at different points throughout the shaft appears to allow the bending behaviour of the shafts to be controlled, whilst also controlling the overall flexural rigidity.

5.2.4.2 Dynamic drop-ball flexure

The shafts behaved very similar dynamically to their static strain distribution. Following the trends of maximum strain points in the multiple sectioned shafts, on the seams between sections and decreasing from the clamp in shaft C 0 (Fig. 6.15). There was not as large a difference between the strain behaviour of shafts V 2 and 4 when tested dynamically. Shaft V 4 did still have a larger increase in strain from 0.05 m to 0.1 m but the increase was half of that evident in quasi-static testing

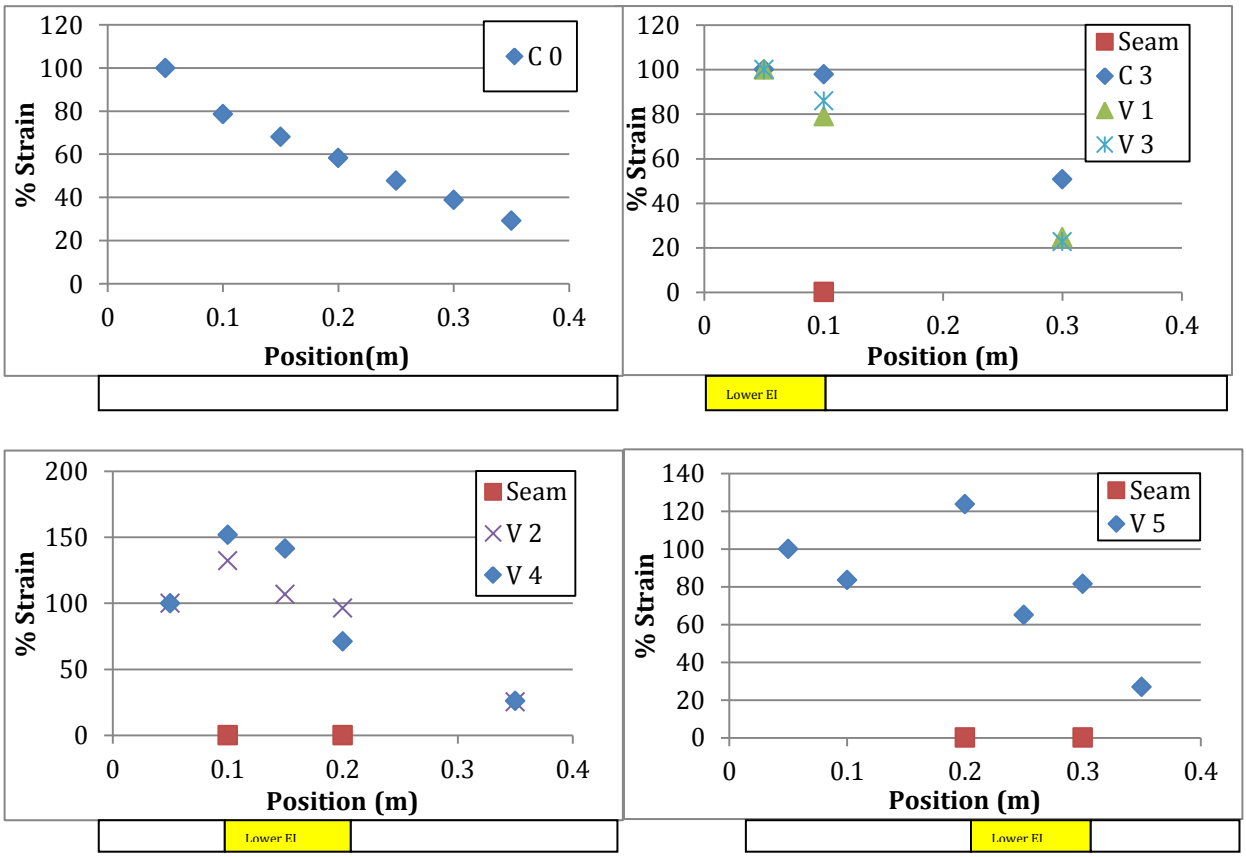

Figure 6.15 – Percentage strain as a function of distance from the clamp in shafts C 0, C 3 and V 1-5 under dynamic deflection. With reference to seam's and lower EI sections.

In order to directly compare the behaviour of the shafts statically and dynamically the percentage strain as a function of distance from the clamp for static (a) and dynamic (b) flexure is shown in Fig. 6.16.

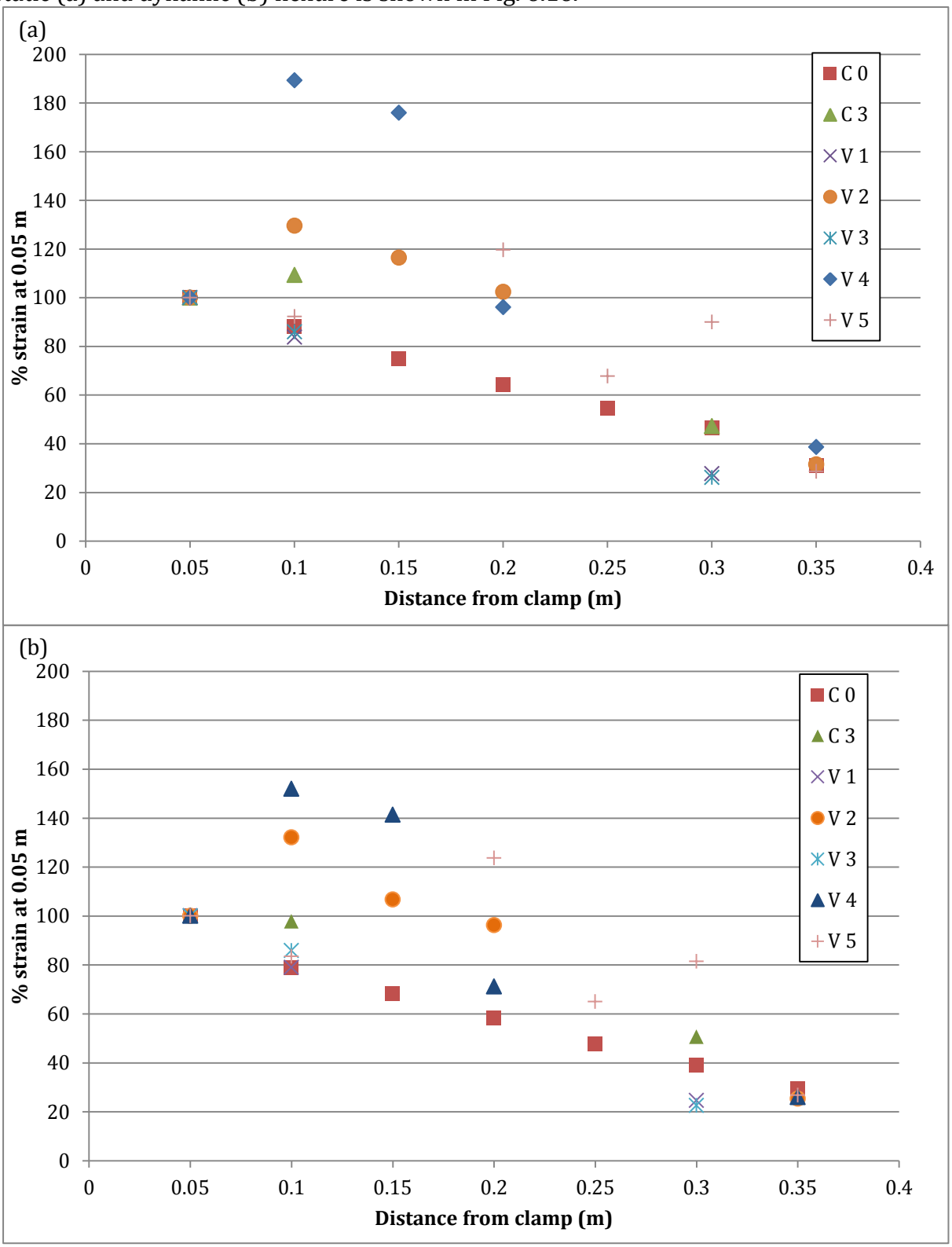

Figure 6.16 - Percentage strain as a function of distance from the clamp in static (a) and dynamic (b) bending.

5.2.4.3 Frequency analysis

By using the 1st natural mode of vibrating frequency obtained from the strain gauge data by analysing the period between peaks, the inverse of this being the frequency (ƒ = 1 / Λ), the respective modulus of the shafts was derived. The behaviour of the control shaft C 0 (a) and a multiple sectioned shaft V 4 (b) is show in Fig. 6.17. The difference in the maximum strain between the shafts is clear to see and the second mode of bending can also be noticed in the data of strain most predominantly furthest away from the clamp.

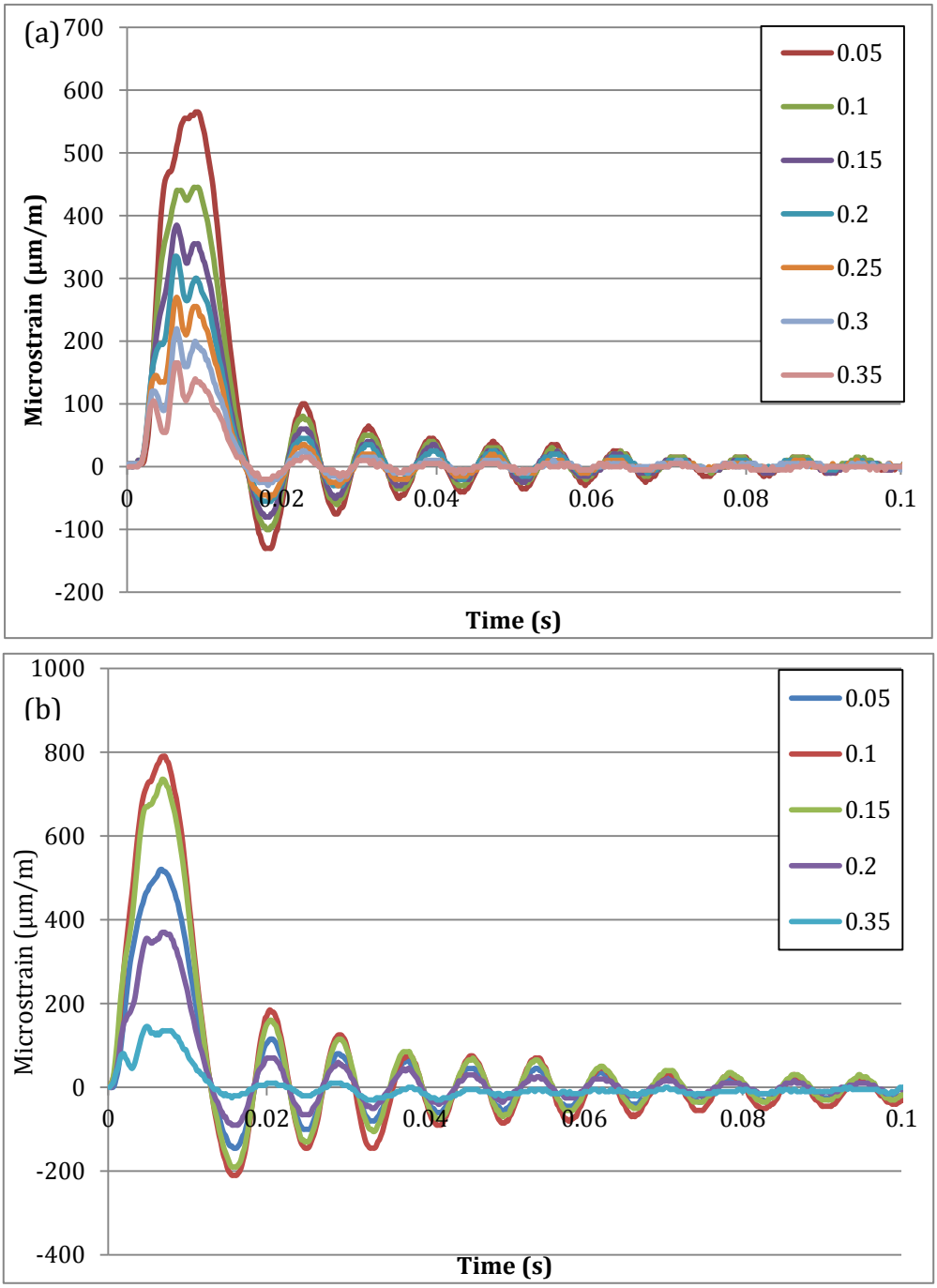

Figure 6.17 – Microstrain as a function of time for increasing distances away from the clamp, showing first and second bending modes in C 0 (a) and V 4 (b).

The modulus obtained from the shafts through this method was consistently higher than that derived from the high speed camera and follows those obtained by static testing closely. Suggesting that the data acquired from the high speed camera in terms of impact force and deflection conversion to modulus was not accurate, or reliable enough because of the use of average force and maximum deflection in the calculations. (Fig. 6.18).

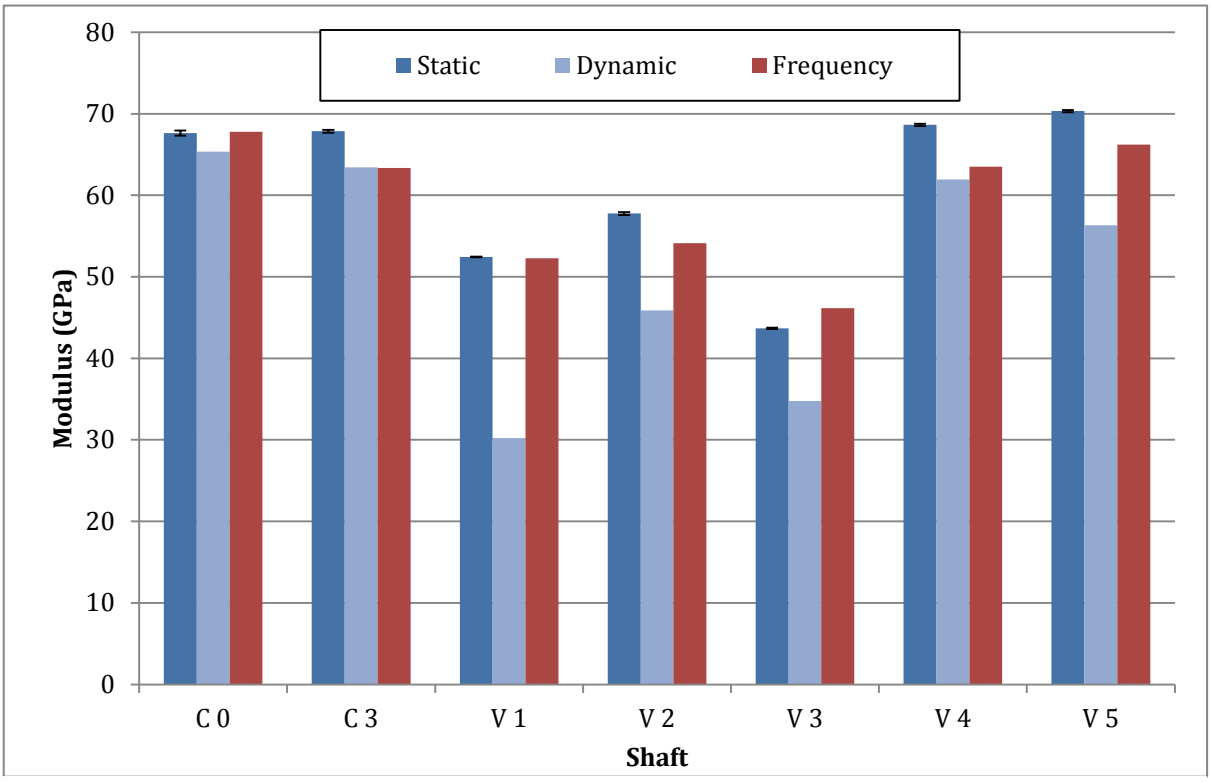

Figure 6.18 – The modulus obtained for shafts C 0, C 3 and V 1-5 by static, dynamic and frequency analysis methods in comparison to CoDA predicted values.

Ignoring shaft V 3, in all methods of testing there is a clear increase in modulus from shaft V 1-5 as was initially modelled. The reason for the anomaly shown in the behaviour of shaft V 3 is not known but will be the focus of microstructural analysis. A discrepancy in the manufacture of the shafts, for example creating an assymmetrical laminate could perhaps have contributed to its poor performance. It has the same section construction as V1 and this does not show a behaviour that was unexpected, in fact these two shaft only have one seam in comparison to the highest modulus shaft V 5 which has two seams. It is interesting that even though the multiple section shafts V 1-5 appear to have underperformed in the dynamic high speed camera tests, however both control shafts, under the same testing conditions show a much better correlation to the other testing scenarios.

5.3 Optical analysis

The ply orientation in shafts V 1-5 is consistent with the intended laminate configurations (Figure 6.19). The average deviation from the intended orientations is shown in Table 6.6 and does not diverge greater than 1.1 degree away from the projected ply angle.

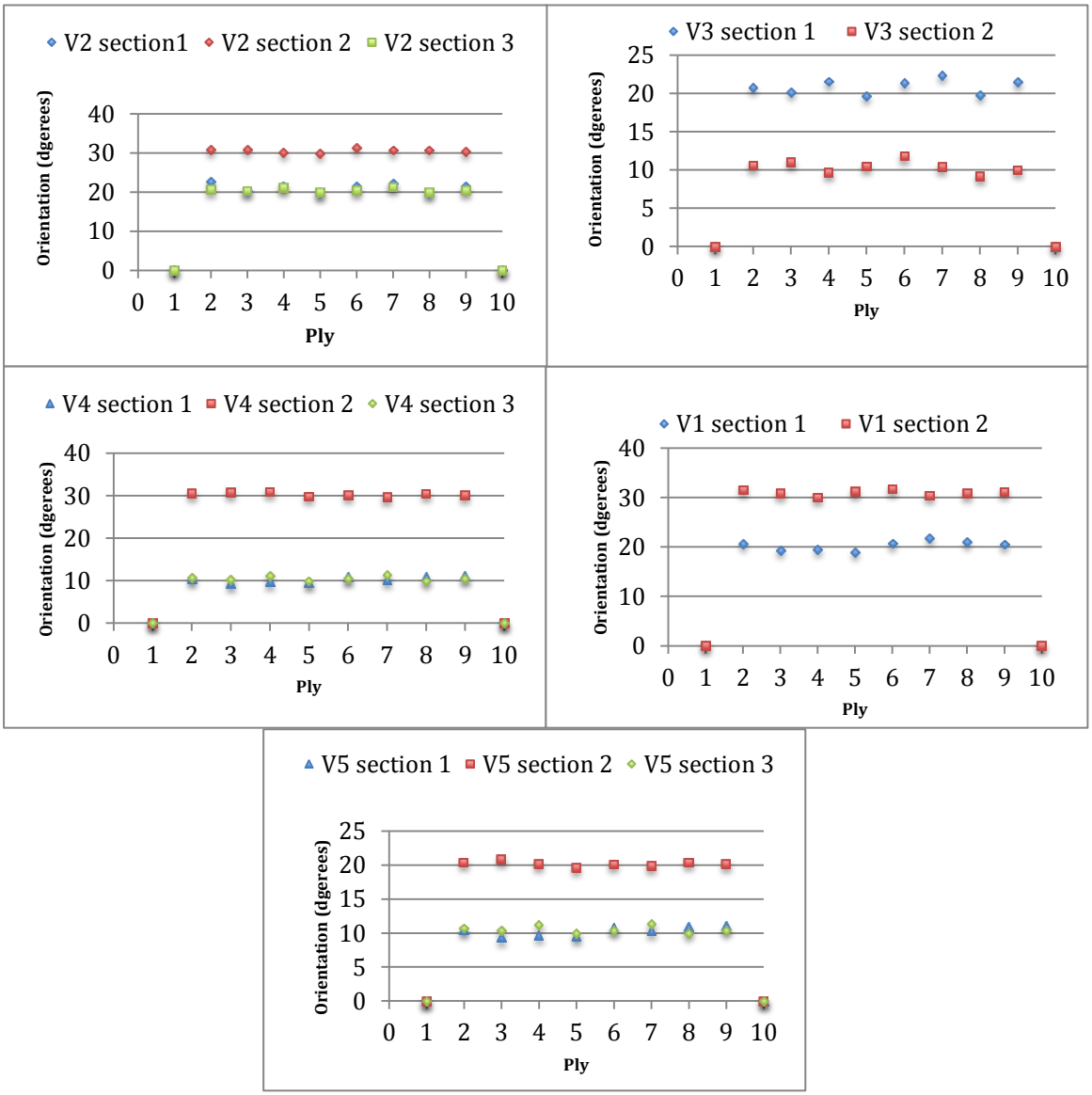

Figure 6.19 – Ply orientation throughout the multiple sections in shafts V 1-5.

The image analysis therefore confirms the accuracy of the hand lay-up technique and shows its consistency through the range of multiple sectioned shafts.

Table 6.6 – Ply orientations and deviation from desired angle for shafts V 1-5.

		Ply											
Shaft	Section	1	2	3	4	5	6	7	8	9	10	Average (°)	Deviation (°)
V 1	1	0	20.7	19.3	19.5	19.0	20.7	21.8	21.0	20.6	0	20.3	0.3
	2	0	31.6	30.9	30.1	31.2	31.7	30.4	30.8	31.2	0	31.0	1.0
V 2	1	0	22.7	20.2	21.6	19.6	21.4	22.3	19.8	21.4	0	21.1	1.1
	2	0	30.8	30.9	30.0	30.0	31.2	30.7	30.7	30.2	0	30.6	0.6
	3	0	20.7	20.4	21.2	19.9	20.4	21.3	19.9	20.4	0	20.5	0.5
V 3	1	0	20.7	20.2	21.6	19.6	21.4	22.3	19.8	21.5	0	20.9	0.9
	2	0	10.6	11.0	9.7	10.5	11.8	10.4	9.2	10.0	0	10.4	0.4
V 4	1	0	10.6	9.3	9.8	9.5	10.8	10.3	10.9	11.0	0	10.3	0.3
	2	0	30.6	30.8	30.9	29.9	30.2	29.7	30.5	30.1	0	30.3	0.3
	3	0	10.7	10.4	11.2	9.9	10.4	11.3	9.9	10.4	0	10.5	0.5
V 5	1	0	10.6	9.3	9.8	9.5	10.8	10.3	10.9	11.0	0	10.3	0.3
	2	0	20.4	20.9	20.1	19.7	20.1	19.9	20.4	20.2	0	20.2	0.2
	3	0	10.7	10.4	11.2	9.9	10.4	11.3	9.9	10.4	0	10.5	0.5

The volume fraction of the multiple sectioned shafts averaged 51.5 % ± 0.6 (Table 6.7), which is ten percent lower than the control shafts. This could be due to the off axis plies not allowing the resin to flow through the laminate under pressing and curing as well as the control 0 degree shaft

Table 6.7 – Volume fraction and cross-sectional area of seams in multiple sectioned shafts V1-5.

	Section Volume fraction (%)				Seam cross sectional area (mm^2)		
Shaft	**1**	**2**	**3**	**Average**	**1/ 2**	**2/ 3**	**Average**
V 1	52.4	51.8		52.1	0.0586		0.0586
V 2	51.7	51.0	51.1	51.3	0.0340	0.0396	0.0368
V 3	51.6	50.3		51.0	0.0542		0.0542
V 4	52.0	52.6	52.0	52.2	0.0283	0.0337	0.0310
V 5	50.0	51.0	51.4	50.8	0.0207	0.0301	0.0254
			Average	**51.5**	**Average**	**0.0412**	
			Stdev	**0.6**	**Stdev**	**0.0145**	

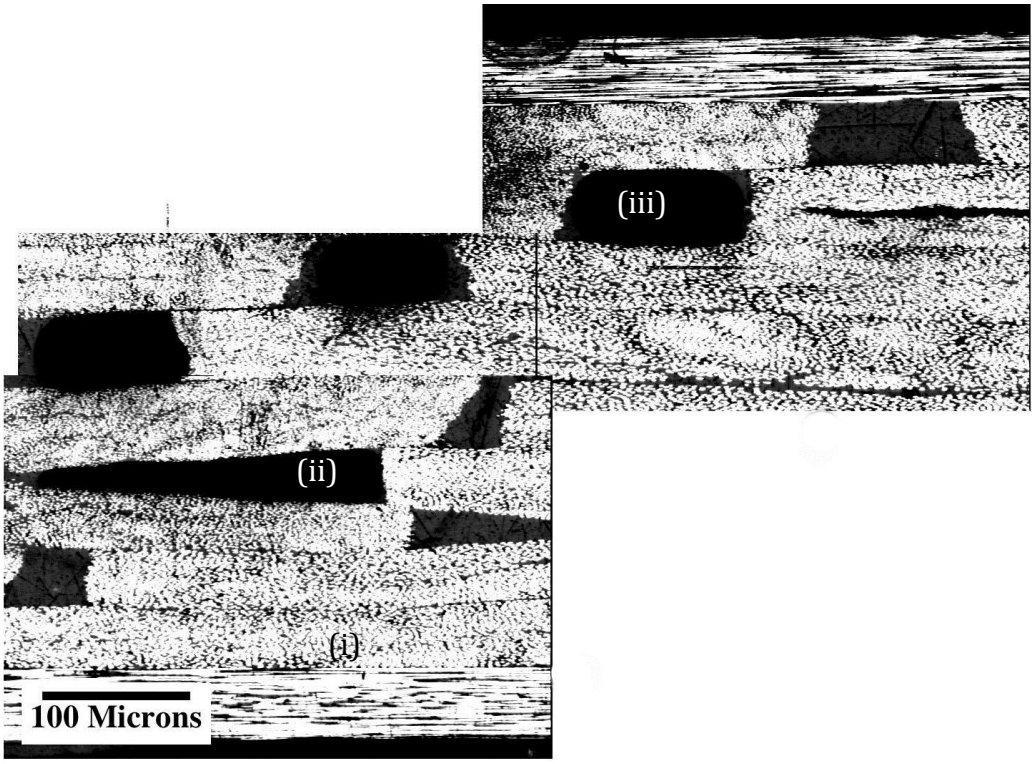

Figure 6.20 – Seam V1 0/30-0/20 examples of good ply interaction (i), ply overlap (ii) and also resin rich regions (iii)

Shaft V1 with a 0.1 m 0/30 section and a 0.4 m 0/20 section only has one seam; the cross-section is shown in Figure 6.20. There are examples of good ply interaction (i), ply overlap (ii) and also resin rich regions (iii) where the plies are not flush with one another. This seam showed the highest overall cross-sectional area of resin rich regions at 0.0586 mm^2. This was the first multiple sectioned shaft to be manufactured with off-axis plies, which added to the complexity of the hand lay-up process.

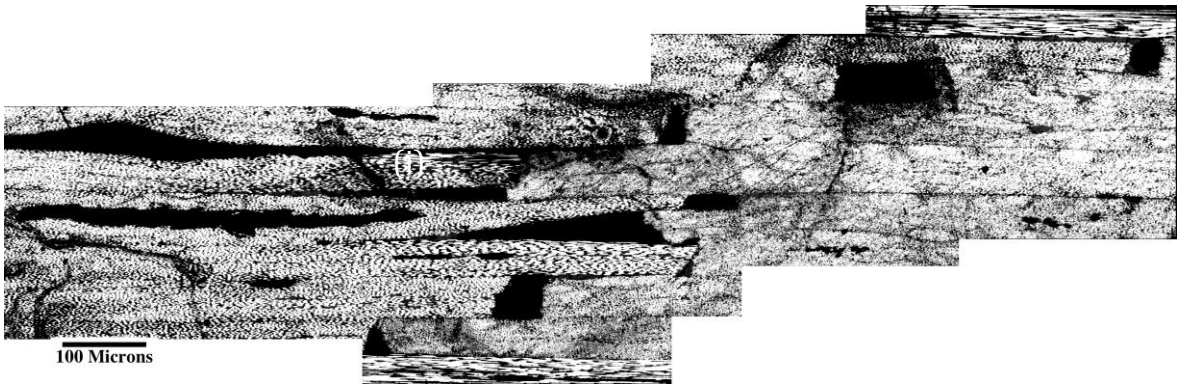

Figure 6.21 – Seam 1 V2, 0/20-0/30. Showing the negative effect of ply overlap. resin rich region extending between plies longitudinally.

The first seam in shaft V2 was the interaction between a 0.1 m 0/20 section and a 0.1 m 0/30 section (Figure 6.21). There is an overall less cross-sectional area of resin at the join between the different orientation plies, in comparison to shaft V1 (0.0340 mm^2). However there are resin rich regions appearing parallel to some of the 0/20 plies in this area. The slight ply overlaps in plies 6/7 has created a path for which the resin has flowed into (i). Suggesting that to overall structure, ply overlap has the most debilitating effect.

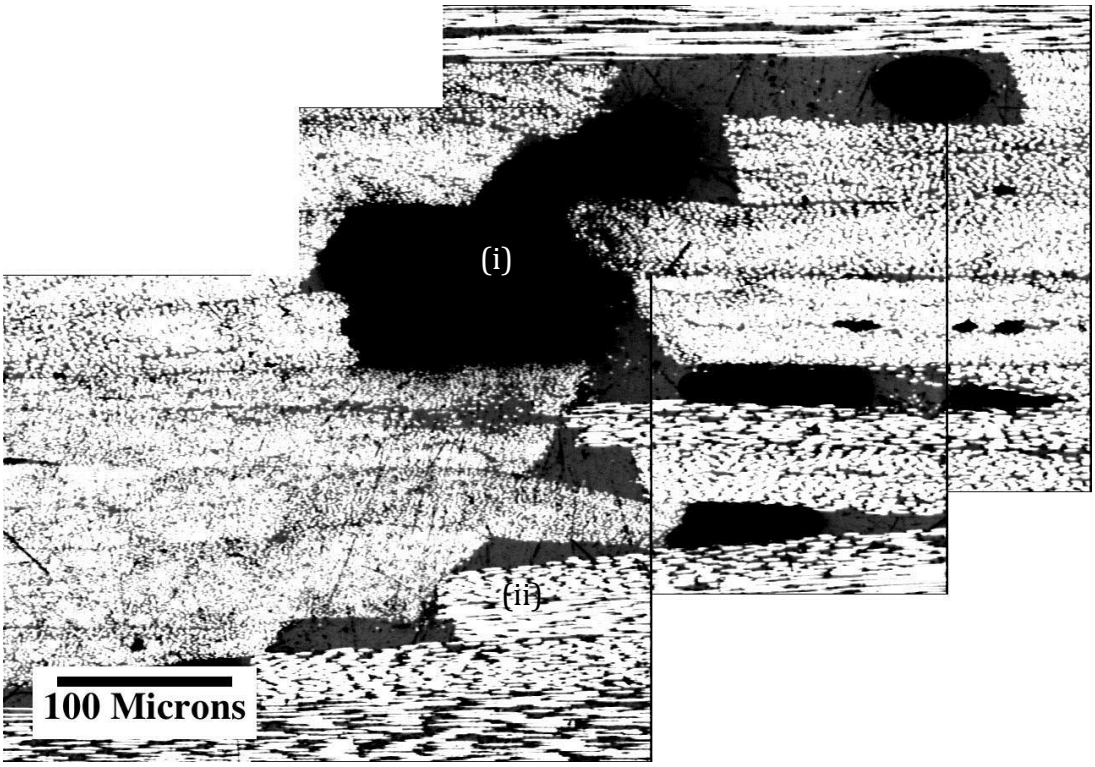

Figure 6.22 – Seam 2, V2 0/30-0/20. Extensive resin- rich region (i) and some ply overlap (ii).

The second seam in shaft V2 is between the 0.1 m 0/30 section and the 0.3 m 0/20 section (Figure 6.22). There is a large resin rich region (i) that dominates the interaction between plies 6-9, however the overall cross-sectional area of the resin rich seam is 0.0396 mm^2, similar to seam 1. There is some ply overlap in plies 2-4 (ii), but it does not have the same effect as was caused in seam 1. The resin rich regions remain localised to the seam.

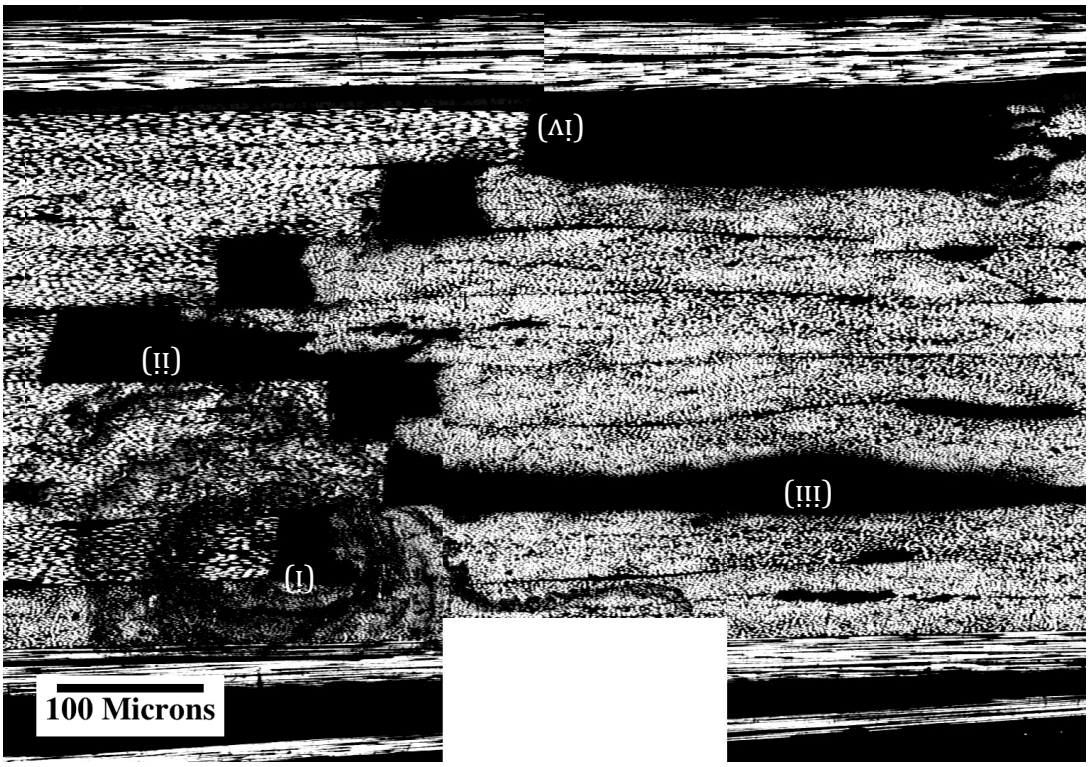

Figure 6.23 – Seam V3 0/20-0/10. Good ply interaction (i), localised resin rich regions (ii), small ply overlap (iii) and a longitudinal resin rich region.

Figure 6.23 shows the interaction between the 0.1 m 0/20 section and 0.4 m 0/10 section in shaft V3. The seam shows some good ply interaction (i),localised resin rich regions (ii) and in ply 4 there is a significant longitudinal resin rich region caused by a small ply overlap (iii). There is also a longitudinal resin rich-region between plies 9 and 10 (iv). The overall cross-sectional area of the resin rich region is the second highest across the shaft range at 0.0542 mm^2. This does not take into account the longitudinal regions, which it was difficult to asses the extent of. The longitudinal resin rich region could help to explain the lower then predicted modulus of this shaft in both static and dynamic conditions. The strain behaviour of the shafts under cantilever loading is dominated by the 0 degree outer plies, as these plies are compromised by a large continuous resin rich region, it follows that the applied force is being transferred by the much lower modulus epoxy resin, not the carbon fibre.

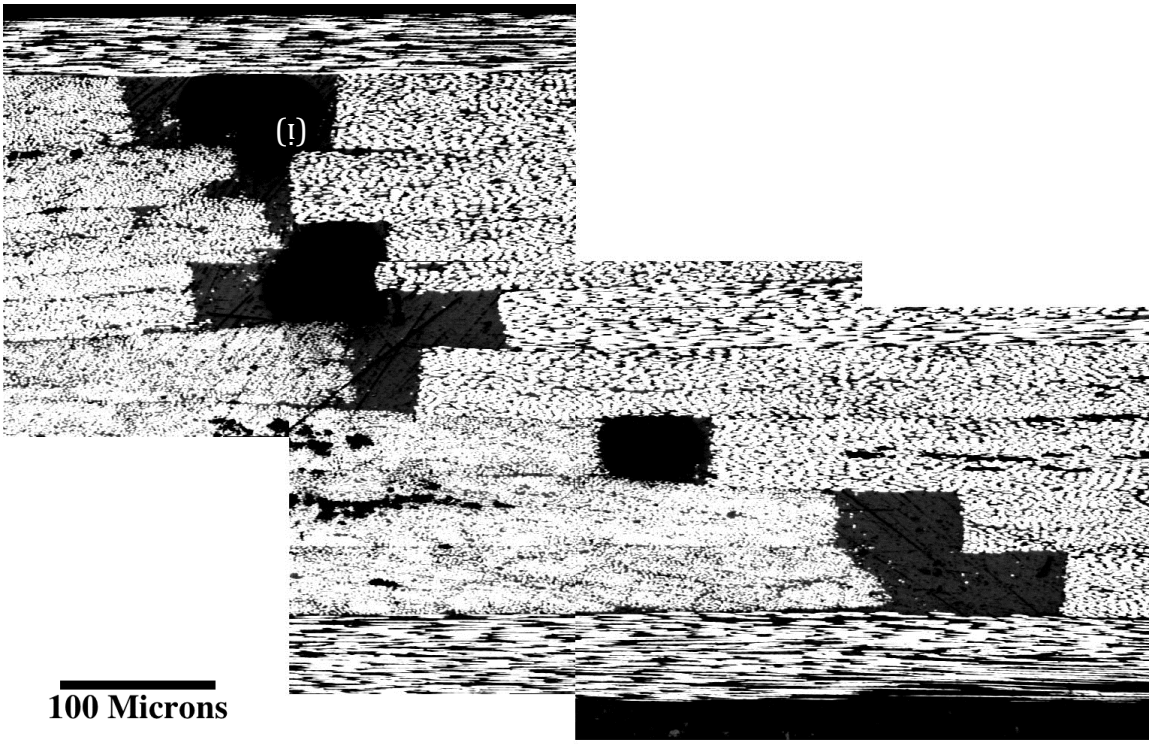

Figure 6.24 - Seam 1, V4 0/10-0/30. Localised resin rich regions (i).

The interaction between the 0.1 m 0/10 section and the 0.1 m 0/30 section is shown on Figure 6.24. There is no ply overlap, as has been the case in previous shafts, which has meant that the resin rich regions are contained at the seam only (i). The overall cross-sectional area of the localised resin rich regions is 0.0283 mm^2, the second lowest across the shafts.

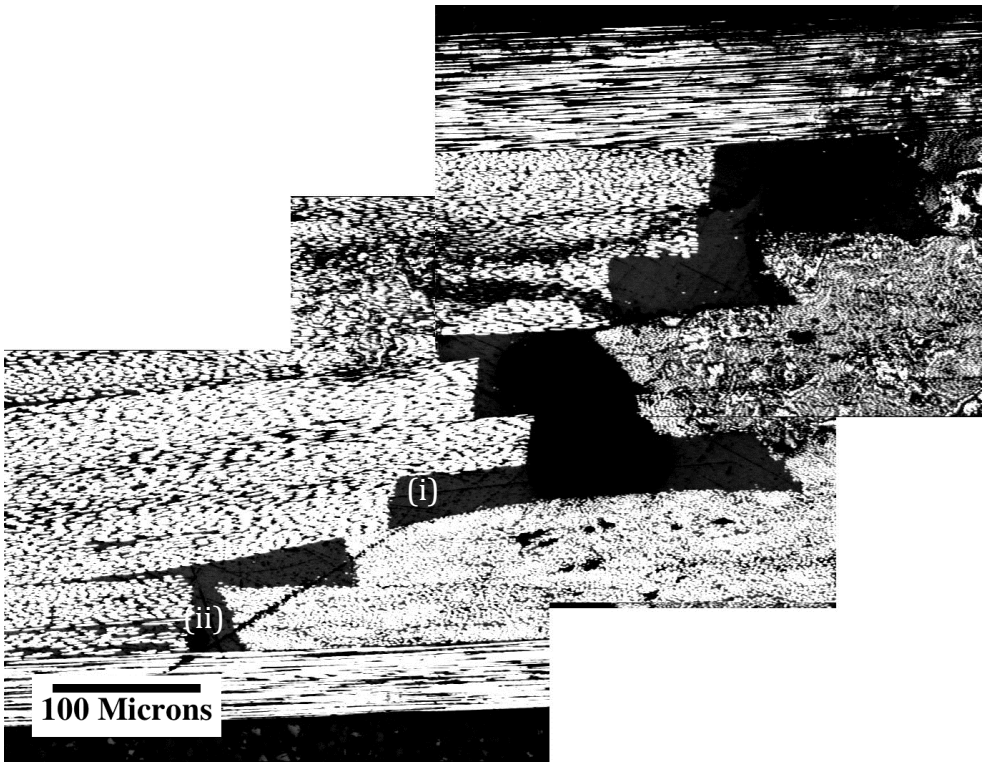

Figure 6.24 – Seam 2, V4 0/30 – 0/10. Ply overlap (i) and localised resin rich regions (ii).

The second seam in shaft V4 is between the 0.1 m 0/30 section and 0.2 m 0/10 section. The interaction is dominated by localised resin rich regions (i). There is also a ply overlap (ii) that has caused a larger resin rich region and some ply distortion in that area. The overall cross sectional area of the resin rich regions was 0.0337 mm^2.

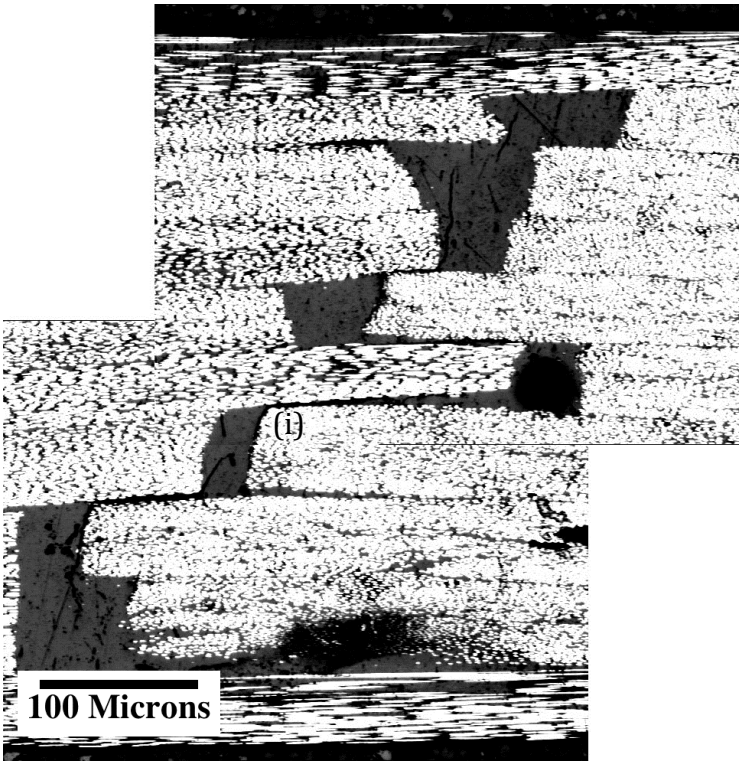

Figure 6.26 -Seam 1, V5 010 – 0/20. Slight ply overlap (i). Resin rich region runs throughout plies 2-9.

The first seam in shaft V5, between 0.2 m 0/10 section and 0.1 m 0/20 section (Figure 6.26) displays a slight ply overlap and some ply distortion (i) and in this seam the resin rich region flows throughout plies 2-9, no localised regions as previously seen. The overall cross-sectional area of the resin rich region is 0.0207 mm^2, even though it flows through all the off-axis plies, the region is the smallest throughout all the shafts and seams.

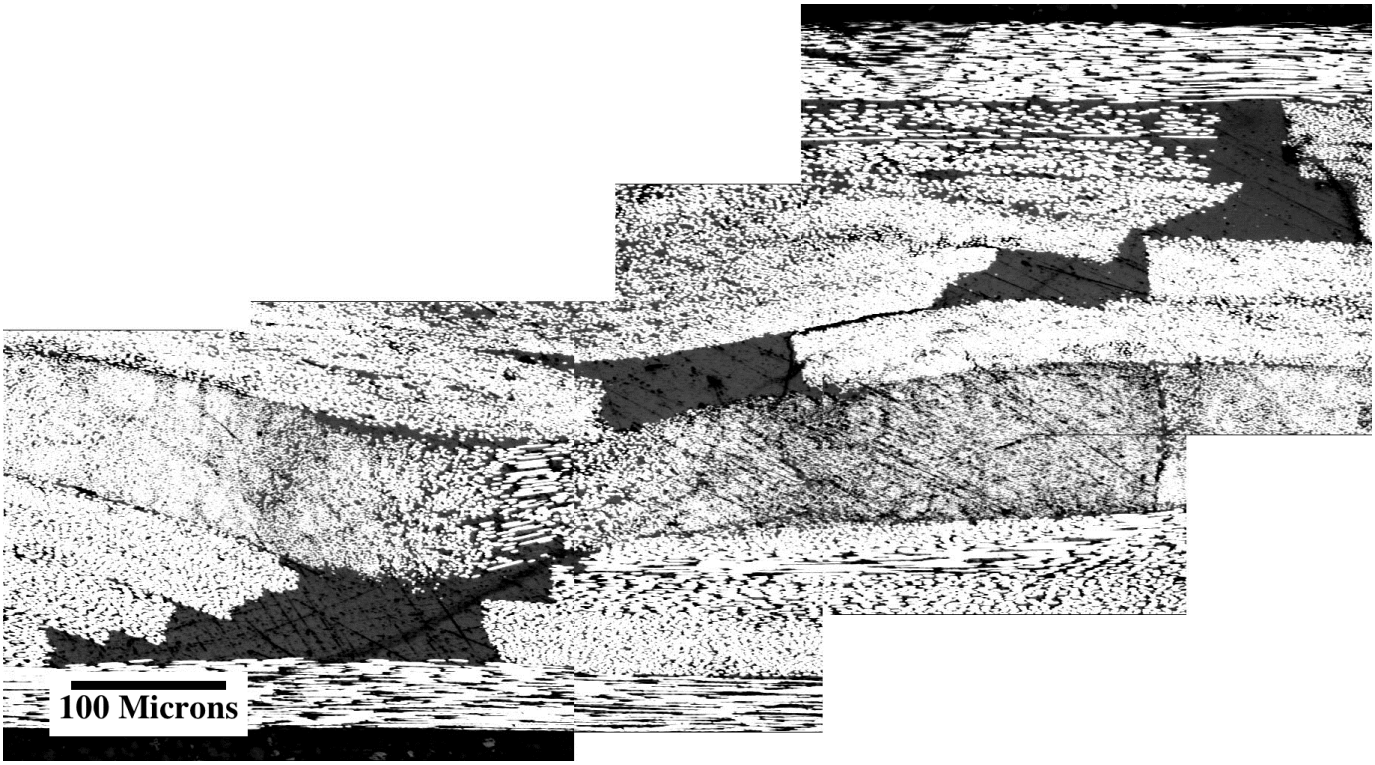

Figure 6.27 – Seam 2,V5 . 0/20 – 0/10. Large resin rich region (i) causes ply distortion throughout the laminate. Localised resin rich regions (ii) and small ply overlap (iii).

The final seam in shaft V5 shown in Figure 6.27, is between the 0.1 m 0/20 section and 0.2 m 0/10. It displays a large resin rich region in plies 2 and 3 which causes ply distortion that runs throughout the laminate, bowing the plies away from parallel (i). There is also some localised resin rich regions (ii) and some small ply overlap contributing to some further slight distortion. The overall cross-sectional area of the resin rich regions throughout the ply is 0.0307 mm^2.

6 Conclusions

- Using CoDA and the manipulated Broulliette equation to predict the behaviour of composite shafts with multiple sections gave a good understanding of the trend of behavior that was to be expected, but was not however accurate enough to predict experimental values.
- It is possible to create multiple sectioned CFRP shafts that can be controlled for overall flexural rigidity and also strain distribution or “kick-point”.
- The hand lay-up and hot pressing technique produces consistent volume fraction and accurate fibre orientation, however the seams at which the sections join requires further investigation and development to ensure better interaction between sections and reduce resin rich regions and ply overlap.
- Validating previous research into the relationship between stick stiffness and ball speed, stiffer shafts produced a higher CoR in the drop ball test.
- There is scope to introduce this control of the bending behavior into hockey sticks by controlling the stiffness along the stick, by either material properties or section moment of area.

7 References

BROULLIETTE, M. (2002) On measuring the flexural rigidity distribution of golf shafts. IN E.THAIN (Ed.) *Science and Golf IV: Proceedings of the fourth world scientific congress of golf.* St. Andrews, Routledge.

CARLISLE, G. (2009) The Design, Construction and Testing of a Controllable Robot to Swing a Hockey Stick. Bsc thesis. *Department of Metallurgy and Materials.* The University of Birmingham.

CHEONG, S. K., KANG, K. W. & JEONG, S. K. (2006) Evaluation of the mechanical performance of golf shafts. *Engineering Failure Analysis,* 13**,** 464 - 473.

COVILL, D., FARR, J., KATZ, T. & WHITE, D. (2008) Use of Static Stiffness Behaviour to Characterise Field Hockey Sticks. IN ESTIVALET, M. & BRISSON, P. (Eds.) *The Engineering of Sport 7.* Biarritz, Springer.

DORÉ, R. & ROY, B. (1976) Dynamometric analysis of different hockey shots. In: *Proceedings of the Fourth International Congress on Biomechanics*, Biomechanics, V-B (ed. Komi, P.V.), pp. 277±285.

FIH (2009) Rules of Hockey, International Hockey Federation (FIH).

HOERNER, E.F. (1989) The dynamic role played by the ice hockey stick. *Safety in Ice Hockey*, ASTM STP 1050 (eds Castaldi, C.R. & Hoerner, E.F.) American Society for Testing and Materials, Philadelphia, PA, 154 -163.

HUNTLEY, M. (2006) Comparison of static and dynamic carbon fibre composite golf club shaft properties and their dependence on structure. *Department of Metallurgy and Materials* The Universtiy of Birmingham.

MATTHEWS, F. L AND RAWLINGS, R. D (1999). Composite materials: Engineering and science. *CRC press. Woodhead publishing Limited.*

MARINO, G. (1998) Biomechanical investigations of performance characteristics of various types of ice hockey sticks. IN RIEHLE & VIETEN (Eds.) *International Society of Biomechanics of Sport.*

MACKENZIE, S. J. (2005) Understanding the role of shaft stiffness in the golf swing. *Phd thesis.* College of Kinesiology, University of Saskatchewan.

MCHUTCHON, M., CURTIS, D. & CARRÉ, M. (2004) Parametric design of field hockey sticks. *The Engineering of Sport 5,* 1**,** 284-290.

MCQUEEN, M. & MCPHEE, J. (2008) Design of an ice hockey test machine. IN M.ESTIVALET & BRISSON, P. (Eds.) *The Engineering of Sport 7.* Biarritz, Springer.

PEARSALL, D. J., MONTGOMERY, D. L., ROTHSCHING, N. & TURCOTTE, R. A. (1999) The infuence of stick stiffness on the performance of ice hockey slap shots. *Sports Engineering,* 2**,** 3-11.

RAI, R. B., G S.; MOHANTY, S K.; GOEL, ANIMESH (2002) Kinematic and Temporal Evaluation of Swings, Stick Length and their Interaction in Field Hockey. *Medicine and Science in Sports and Exercise,* 34**,** 18.

RANGA, D., CORNISH, J. & STRANGWOOD, M. (2008) The Role of Materials and Construction on Hockey Ball Performance. *The Engineering of Sport 7,* 1**,** 457-464.

SMITH, L. V. (2001) Evaluating baseball bat performance, *Sports Eng*. **4**, 205–214.

TSAI, S. W AND HAHN, H. T (1980) Introduction to composite materials.*Technomic publising Co., Inc.*

VAN GHELUWE, B., DEPORTE, E., & BALLEGEER, K. (1990). The influence of the use of graphite shafts on golf performance and swing kinematics. In A. J. Cochran (Ed.), *Science and Golf: Proceedings of the First World Scientific Congress of Golf* (pp. 258-263). United Kingdom: E & FN Spon.